

# Chiral Symmetry Restoration and Deconfinement in Neutron Stars

Dissertation

zur Erlangung des Doktorgrades  
der Naturwissenschaften

vorgelegt beim Institute fuer Theoretische Physik  
der Johann Wolfgang Goethe-Universitaet  
in Frankfurt am Main

von

Verônica Antocheviz Dexheimer  
aus Porto Alegre, Brasilien

Frankfurt am Main, Maerz 2009  
(FB 13)



# Zusammenfassung

Neutronensterne sind Objekte sehr hoher Dichte – ein Teelöffel Ihrer Bestandteile hätte ein Gewicht von ca. fünf Milliarden Tonnen. Die Gravitationskraft auf ihrer Oberfläche ist so stark, dass diese ein fallendes Objekt innerhalb eines Meters auf eine Geschwindigkeit von zweitausend Kilometer pro Sekunde beschleunigen würde. In Objekten solcher hoher Dichte können Teilchen existieren, die sich von den Nukleonen in Atomkernen unterscheiden. Solche Teilchen können Hyperonen mit nichtverschwindender Strangeness sein, oder auch breitere Resonanzen. Weiterhin können in Neutronensternen verschiedenen Materiezustände vorkommen, so zum Beispiel Mesonenkondensate oder auch "Quarkmatter" im Falle einer für das Deconfinement der Nukleonen ausreichenden Dichte. Mit dem Auftreten neuer Freiheitsgrade des Systems müssen verschiedene Eigenschaften der Materie berücksichtigt werden. Der in diesem Zusammenhang wichtigste Aspekt ist die Wiederherstellung der chiralen Symmetrie. Diese Symmetrie ist ansonsten spontan gebrochen, eine Tatsache, die im Zusammenhang mit dem Vorhandensein eines Kondensates von skalaren Quark-Antiquark Paaren steht. Solch ein Kondensat, wegen des eben genannten Zusammenhanges auch chirales Kondensat genannt, tritt bereits im Vakuum auf. An dieser Stelle muss daran erinnert werden, dass im modernen Verständnis das Vakuum alles andere als ein Zustand der "Leere" ist, vielmehr zeichnet es sich durch die Präsenz virtueller Teilchen aus, welche permanent gemäß des Unschärfepinzips erzeugt und vernichtet werden. Bei hohen Temperaturen/Dichten, wenn die zusammengesetzten Teilchen in ihre Konstituenten aufgelöst werden, verschwindet das chirale Kondensat und die chirale Symmetrie ist wiederhergestellt.

Um erklären zu können, wie und zu welchem Zeitpunkt die chirale Symmetrie in Neutronensternen wiederhergestellt wird, benutzen wir ein als Sigma-Omega-Modell bezeichnetes effektives relativistisches quantenmechanisches Modell. Dieses Modell wurde zur Beschreibung von Systemen entwickelt, die aus über Mesonen wechselwirkenden Baryonen bestehen. Es wurde von Symmetrierelationen ausgehend konstruiert, wodurch das Modell chiral invariant ist. Die erste Konsequenz dieser Invarianz ist die

Tatsache, dass in der Lagrangedichte keine reinen Massenterme auftreten, wodurch alle, oder zumindest die meiste, Teilchenmasse aus der Wechselwirkung mit dem Medium resultiert.

Neutronensterne weisen noch weitere Besonderheiten auf, die sonst nirgends in der Natur gefunden werden koennen. Eine dieser Besonderheiten ist die Isospin-Asymmetrie: In gewoehnlichen Atomkernen ist die Anzahl der Neutronen und Protonen ungefaehr gleich, waehrend in Neutronensternen sehr viel mehr Neutronen als Protonen vorhanden sind. Durch dieses asymmetrische Verhaeltnis wird die Energie des Systems um einen als Fermi-energie bezeichneten Betrag erhoehrt, was eine erhoehrte Masse des Sternes erlaubt. In fruehen Phasen der Sternentwicklung, wenn noch viele Neutrinos im Stern gebunden sind, ist das Verhaeltnis von Protonen zu Neutronen hoeher als zu spaeteren Phasen der Entwicklung. Folglich ist in diesen fruehen Phasen die Masse, die der Stern gegen die Gravitation aufrechterhalten kann, vergleichsweise geringer. Nicht nur in diesem Kontext zeigt sich, wie die Phaenomene auf mikroskopischer Ebenes im Zusammenhang mit den makroskopischen Eigenschaften des Sternes stehen. Ein weiteres Charakteristikum eines Neutronensterns ist die Ladungsneutralitaet. Diese ist eine, aber nicht die einzige, notwendige Voraussetzung fuer die Stabilitaet des Sternes. Ein weiteres Beispiel ist das chemische Gleichgewicht. Dieses muss nicht notwendigerweise bedeuten, dass die Anzahl jeder Art von Teilchen erhalten ist, jedoch dass die Teilchen durch spezifische Reaktionen erzeugt und vernichtet werden, die in beide Richtungen mit gleicher Rate erfolgen.

Obwohl zur Beschreibung der mikroskopischen Physik von Neutronensternen die Raumzeit der speziellen Relativitaetstheorie, d.h. der Minkowski Raum, benutzt werden kann, trifft dies nicht auf die makroskopischen Eigenschaften des Sternes zu. Fuer diese muss eine Beschreibung im Rahmen der allgemeinen Relativitaetstheorie gewaehlt werden, welche die Gravitation mitberuecksichtigt. Die Loesungen der Einsteinschen Feldgleichungen fuer den vereinfachten Fall statischer, sphaerischer und isotroper Sterne entsprechen der Konfiguration eines hydrostatischen Gleichgewichtes. In diesem Gleichgewicht verhindert eine Balance zwischen dem hauptsaechlich aus der Fermi-Energie der Baryonen und Leptonen resultierenden inneren Druck und der Gravitationskraft den Kollaps des Sternes. Im Falle einer Rotation verstaerkt sich die Stabilitaet des Sternes, was eine erhoehrte Masse desselben ermoeglicht. Die Rotationsbewegung hebt die sphaerische Symmetrie auf, wodurch die Metrik des Sternes eine Funktion in Ab-

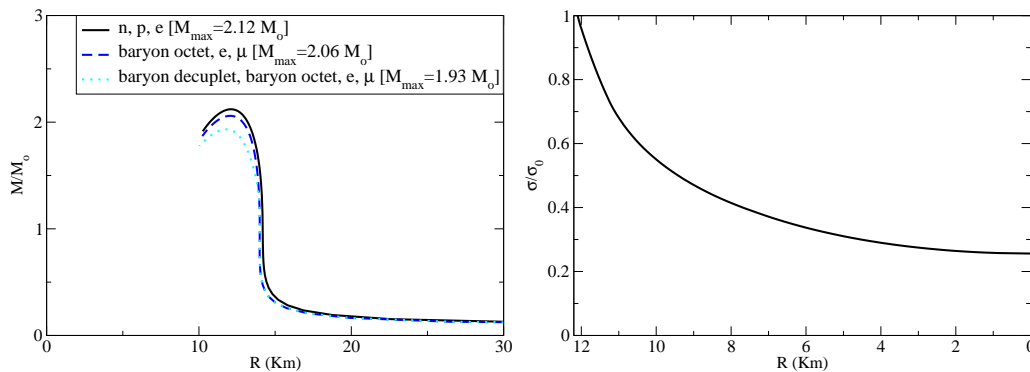


**Figure 0-1:** Links: Masse-Radius-Diagramm fuer Sterne mit verschiedenen baryonischen Freiheitsgraden (gezeigt werden die Werte der jeweiligen hoechsten Masse). Rechts: Skalares Kondensat gegen den Radius des Sterns.

haengigkeit von der Polarkoordinate wird. Weiterhin muss der Einfluss des lokalen Bezugssystems mitberuecksichtigt werden. Dieses erzeugt Zentrifugalkraefte, welche nicht der Wechselwirkung mit anderen Koerpern entstammen, sondern im Zusammenhang mit dem Bezugssystems des Beobachters stehen, welches im Gegensatz zum Stern nicht rotiert. Diese Aspekte werden durch Stoerungsrechnungen im Rahmen der Sogenannten Hartleschen Naehering beruecksichtigt.

In der "Mean Field" Naehering erfolgt eine Anpassung der Kopplungen sowie der Parameter des Sigma Modells derart, dass massive Neutronensterne reproduziert werden koennen. Der linke Teil von Fig. 0-1 zeigt wie die Einfuehrung neuer Freiheitsgrade die maximal erlaubte Masse des Neutronensternes reduziert. Bei den berechneten Sternen sind die einzigen Baryonen, die neben den Nukleonen im Stern vorhanden sind, im Falle der Integration des Baryonen Oktetts die  $\Lambda$  und  $\Sigma^-$ , und im Falle der Integration des Baryon Dekuplett die  $\Lambda$  und  $\Delta$ -Resonanzen. Die Leptonen wurden zur Sicherstellung der Ladungsneutralitaet eingefuehrt. Um Unsicherheiten in den Kopplungen zu vermeiden, wurden in den weiteren Berechnungen das Baryon-Oktett und nicht das Baryon-Dekuplett beruecksichtigt. Die Kopplungen der Hyperonen wurden gemaess der Tiefe ihrer Potentiale in Hyperkernen gefittet. In diesem Fall kann die Wiederherstellung der chiralen Symmetrie anhand des Verhaltens des Ordnungsparameters beobachtet werden. Der rechte Teil von Fig. 0-1 zeigt, dass die Wiederherstellung der Symmetrie in Neutronensternen beginnt, und dass bei diesem Uebergang eine gleichmaessige Aenderung auftritt.

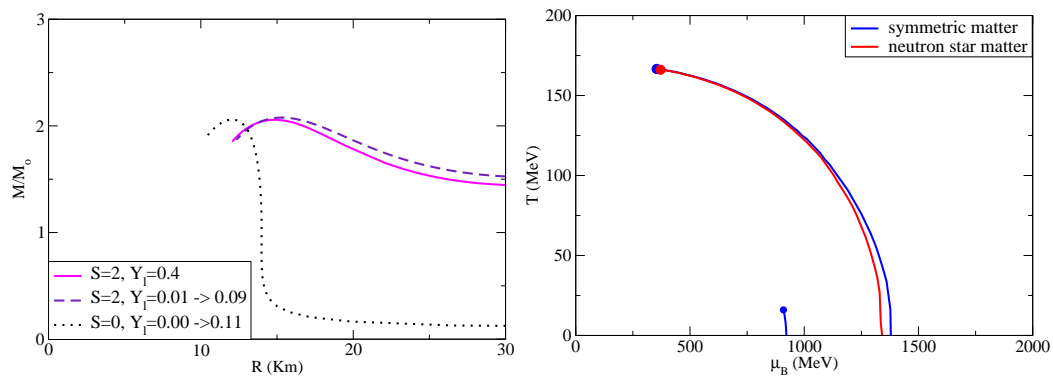


**Figure 0-2:** Links: Masse des Sterns in verschiedenen Phasen der Sternentwicklung, definiert durch die Entropie und die Leptonenzahl unter Berücksichtigung des Baryonen-Oktetts,  $e$ ,  $\mu$ . Rechts: Phasendiagramm der Materie in der Ebene von Temperatur und baryonischen chemischen Potential, die Linien repräsentieren Phasenübergänge erster Ordnung für isospin-symmetrische und Sternmaterie, die Kreise markieren die jeweiligen kritischen Punkte.

Unter Einschluss gebundener Neutrinos, endlicher Temperaturen und der Entropie werden verschiedene Phasen der Sternabkühlung reproduziert. Berechnungen mit endlicher Temperatur beinhalten das Wärmebad der hadronischen Quasi-Teilchen innerhalb des Grosskanonischen Potentials des Systems. Verschiedene Schemata werden berücksichtigt, welche konstante Temperatur, metrikabhängige Temperatur und konstante Entropie beinhalten. Das chemische Potential der Neutrinos wird mittels Festsetzung der Leptonenzahl eingeführt, wodurch aufgrund der Ladungsneutralität auch die Anzahl der Elektronen und Protonen kontrolliert wird. Isolierte Sterne haben eine feste Anzahl von Baryonen, wodurch verschiedene Phasen des Abkühlungsprozesses miteinander verbunden sind. Der linke Teil von Fig. 0-2 zeigt die maximal erlaubte Masse in den verschiedenen Phasen des Abkühlungsprozesses, d.h. der Phase mit hoher Entropie und gebundenen Neutrinos, der Phase ohne Leptonen mit hoher Entropie und der kalten Phase im Beta-Gleichgewicht.

Der Abkühlprozess wird auch durch Nebenbedingungen beeinflusst, die aus der Rotation des Sternes resultieren. Durch diese erreicht der Stern eine höhere Stabilität und demzufolge ebenso eine höhere Masse. Die Rotationsbewegung deformiert den Stern, wodurch Modifikationen der zugehörigen Metrik erforderlich werden, in unserer Berechnung durch Störungstheorie realisiert. Die Analyse der ersten Phasen des

Neutronensterns, in welchen dieser Proto-Neutronenstern genannt wird, führt zu Einschränkungen der möglichen Rotationsfrequenzen während der kälteren Phasen. Es werden Instabilitätsfenster berechnet, in denen der Stern zwar während einzelner Phasen stabil ist, aber im Verlauf des Abkühlprozesses in ein Schwarzes Loch kollabiert.

Im letzten Teil dieser Arbeit wird das hadronische  $SU(3)$  Modell in dem Sinne erweitert, dass es zu den Quarks zugehörige Freiheitsgrade beinhaltet. Hierbei verknüpft ein neues effektives Potenzial für den zum Deconfinement gehörenden Ordnungsparameter, die Polyakov-Schleife, die Physik bei niedrigem chemischen Potenzial und hoher Temperatur im QCD Phasendiagramm mit dem Bereich hohen chemischen Potenzials und niedriger Temperatur. Durch das Studium der Auswirkungen auf die beiden Ordnungsparameter, das chirale Kondensat und die Polyakov-Schleife, ist es uns möglich, ein Phasendiagramm sowohl für isospin-symmetrische wie auch ladungsneutrale Sternmaterie zu erzeugen. Der rechte Teil in Fig. 0-2 zeigt, dass das Diagramm einen Übergangsbereich enthält, sowie eine Linie eines Phasenübergangs erster Ordnung. Die neuen Kopplungen und Parameter des Modells sind weitestgehend gemäß einer Übereinstimmung mit Gitter-QCD-Ergebnissen gefittet, dies beinhaltet auch die Position des sogenannten Kritischen Endpunkts. In Abhängigkeit davon, welcher Teil des Phasendiagramms betrachtet wird, sind verschiedene Freiheitsgrade relevant. Letztlich werden mit Hilfe dieser Methoden Eigenschaften von Hybridsternen berechnet, die sowohl aus Baryonen als auch Quarks bestehen.





# Contents

<b>Zusammenfassung</b>	<b>3</b>
<b>Contents</b>	<b>9</b>
<b>1 Introduction</b>	<b>13</b>
<b>2 The Nonlinear Realization of the Sigma Model</b>	<b>21</b>
2.1 Symmetries . . . . .	22
2.2 Anomalies . . . . .	25
2.3 Construction of the Model . . . . .	26
2.4 The Nonlinear Realization of the Sigma Model . . . . .	30
2.4.1 Kinetic energy term . . . . .	30
2.4.2 Interaction term between baryons and mesons . . . . .	31
2.4.3 Self interaction term for the spin-0 mesons . . . . .	34
2.4.4 Self interaction term for the spin-1 mesons . . . . .	35
2.4.5 Explicit symmetry breaking term . . . . .	36
2.5 Mean Field Theory Approximation . . . . .	37
<b>3 Neutron Stars</b>	<b>41</b>
3.1 Star Matter . . . . .	41
3.2 Inclusion of Gravity . . . . .	43
3.3 Different Couplings . . . . .	45
3.4 Different Compositions . . . . .	46
3.5 Chiral Symmetry Restoration . . . . .	48
<b>4 Proto-Neutron Stars</b>	<b>51</b>
4.1 Finite Temperature . . . . .	51
4.1.1 Constant temperature . . . . .	52
4.1.2 Metric dependent temperature . . . . .	53

---

4.1.3	Constant entropy . . . . .	53
4.2	Trapped Neutrinos . . . . .	54
4.3	Cooling Stages . . . . .	55
4.4	Meson Condensation . . . . .	59
<b>5</b>	<b>Rotational Effects</b>	<b>63</b>
5.1	Formalism . . . . .	63
5.2	Kepler Frequency . . . . .	65
5.3	Modification on Stars . . . . .	66
5.4	Constraints for the Cooling . . . . .	67
<b>6</b>	<b>Hybrid Stars</b>	<b>69</b>
6.1	Motivation . . . . .	69
6.2	The Modified Model . . . . .	70
6.3	The Phase Diagram . . . . .	72
6.4	Hybrid Stars . . . . .	74
6.4.1	Local charge neutrality . . . . .	74
6.4.2	Global charge neutrality . . . . .	76
6.5	Degrees of Freedom . . . . .	77
6.6	Isotherms and Isentropes . . . . .	80
<b>7</b>	<b>Conclusion and Outlook</b>	<b>83</b>
<b>8</b>	<b>Apendix</b>	<b>87</b>
	<b>Bibliography</b>	<b>87</b>
	<b>References</b>	<b>89</b>
	<b>List of Figures</b>	<b>95</b>
	<b>List of Tables</b>	<b>97</b>
	<b>Acknowledgments</b>	<b>99</b>
	<b>Publications</b>	<b>101</b>

**Contents**

**11**

---

**Curriculum Vitae**

**103**



# 1 Introduction

Neutron stars are the densest objects existing in nature. Although black holes are even denser than neutron stars, these objects are singularities [1] and, for this reason, not much can be said about their interior. Neutron stars, on the other hand, emit radiation in a very special way due to their extremely high magnetic field and rotation. This combination leads the star to emit radiation along the direction of the magnetic axis, that can be seen once every rotation for an observer lying in the direction of the beam (Fig. 1-1). Because of this mechanism, that works essentially as a lighthouse, these objects were named pulsars. Since the discovery of the first pulsar, made by Jocelyn Bell in 1967 [2], many others were discovered. It is believed that there are over 30.000 pulsars inhabiting our galaxy.

Many properties of pulsars can be observed or inferred from measurements. The most trivial one is the rotation frequency, that was found to lie between 1 time and 716 times per second [3]. At this incredible rate the particles at the outer part of the star are moving at one fourth of the speed of light. Radii and masses, which are the most important parameters used to calibrate and select between models that describe these stars, can also be estimated with a reasonable precision, especially from the pulsars in binary systems. One very interesting characteristic of binary stars, is that the analysis of their orbits can be used to prove General Relativity up to a 0.05% level [4].

Even more impressive than neutron stars are the explosions that create them. They are called supernovae and happen in our galaxy approximately once per thirty years. In a few seconds these explosions release the brightness of thousands of suns, reaching in the peak the impressive brightness of millions of suns. It is not surprising that such a phenomenon has been observed since ancient times. The first one was documented in 1054 and created the famous Crab Nebula [5] (Fig. 1-2). It is a cloud of gas and dust of 10 light years across illuminated by a pulsar. But supernovae are not only interesting for their beauty. Their redshift can be used to show that the universe is expanding and it is doing so at an accelerating rate. This is done by measuring the relativistic effect of the increase or decrease of the radiation frequency of the approaching or receding

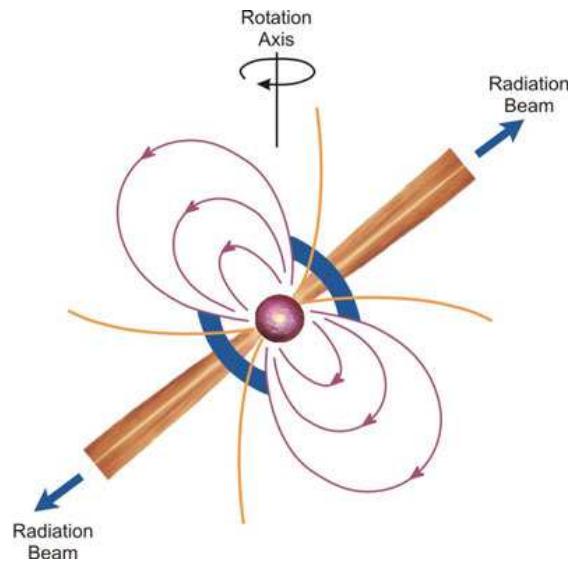


**Figure 1-1:** *Pulsar mechanism*

star [6]. Besides that, the detection of the neutrinos emitted during the explosion can reveal much about the physics happening in the star interior and about the properties of the neutrinos themselves.

Above all, the most amazing fact about supernovae is that they are essentially responsible for the creation of life. Typically in our universe, only light atoms like hydrogen or helium are found. All the heavier elements (lighter than iron) are generated inside heavy stars, that spread them throughout all the universe during these explosions. The atoms heavier than iron are created in a later stage, just outside the newly formed neutron star due to the intense neutrino bombardment. About  $2/3$  of the matter around us is made by the first stars that appeared approximately 200.000 years after the beginning of the universe. This relates to the fact that those stars were much heavier than the ones that exist nowadays, which made their whole evolution happen faster (bigger stars radiate more energy). The younger and lighter stars are still on the main sequence of their evolution.

The whole evolution process of stars happens independently of the exterior (within the limits of this being possible while exchanging energy with the medium) but for the initial stage. At this point, the interstellar cloud can start to contract and become a proto-star only if there is a perturbation of a certain wavelength, higher than the

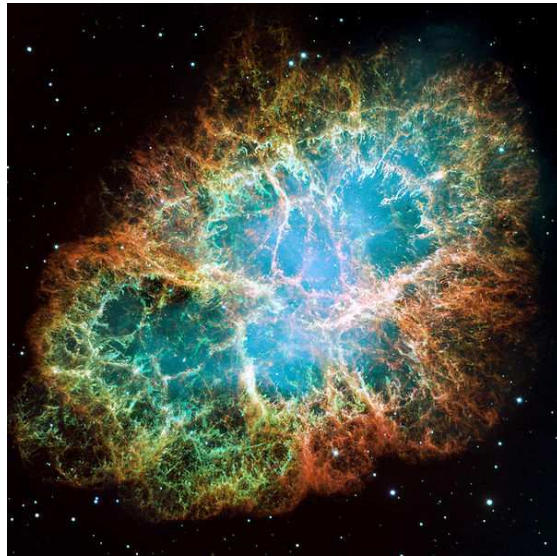


**Figure 1-2:** *Crab nebula*

so called Jeans length [7]. These perturbations are in general caused by shock waves proceeding from supernovae. In this sense, these explosions not only create the elements necessary for life, but also help to form new stars, and also planets, containing these elements.

The process that leads to the supernova is the following. After spending most of its time in the so called "main sequence", converting hydrogen into helium, the star proceeds producing heavier and heavier elements (He, C, O, Ne, Mg, Si, S) until iron, the element with the highest binding energy per nucleon (Fig. 1-3). After that, the fusion process is not exothermic and consumes instead of releasing energy into the system. Without the thermal energy, used to balance the star against gravity, it starts to collapse forming two distinct regions, a homogeneously collapsing inner core and a free falling outer one. After the inner core becomes dense enough for the strong nuclear force to come into play, the extra pressure coming from it stops the collapse in this region and generates a pressure wave that dissolves the nuclei into nucleons. When this wave reaches the boundary of the outer region, it becomes a shock wave that travels outside the star and, through very complicated mechanisms [8], ends up expelling most of the mass of the star leaving behind a small object of just tens of kilometers called neutron star.

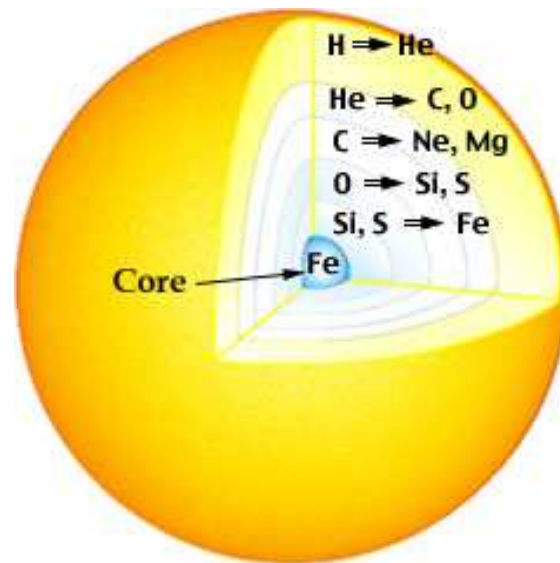


**Figure 1-3:** *Main sequence star structure*

In such dense objects different particles, more massive than nucleons, can exist. These particles can be hyperons, that contain non-zero strangeness, or broader resonances, that become stable as their decay is Pauli-blocked in the dense system. There can also be different states of matter inside neutron star, such as meson condensates, and if the density is high enough to deconfine the nucleons, quark matter. As new degrees of freedom appear in the system, different aspects of matter have to be taken into account, the most important of them being the restoration of the chiral symmetry. This symmetry is spontaneously broken, which is a fact related to the presence of a condensate of scalar quark-antiquark pairs, that for this reason is called chiral condensate. This condensate is present at low densities and even in vacuum. It is important to remember at this point that the modern concept of vacuum is far away from emptiness. It is full of virtual particles that are constantly created and annihilated, their existence being allowed by the uncertainty principle. At very high temperature/density, when the composite particles are dissolved into constituents, the chiral condensate vanishes and the chiral symmetry is restored. To explain how and when this phenomenon happens inside neutron stars is the main scope of this work and the topic will be explored in the next chapters.

There are still other interesting features in neutron stars that cannot be found



anywhere else in nature. One of them is high isospin asymmetry. In normal nuclei, the number of protons and neutrons are more or less the same. In a neutron star the number of neutrons is much higher than the one of protons. This provides extra Fermi energy, raising the energy of the system and allowing the star to support more mass against gravitational collapse. Enrico Fermi showed that for spin half particles, there can be two of each kind (one with spin up and one with down) in each state. For this reason systems with high particle degeneracy have less occupied energy levels. For example, in early stages of the neutron star evolution, when there are still many trapped neutrinos, the proton fraction is higher than in later stages and consequently the maximum mass that the star can support against gravity is smaller. This, among many other features, shows how the microscopic phenomena in the interior of the star are reflected in its macroscopic properties.

Another important property of neutron stars is charge neutrality. These objects have to be charge neutral to be stable and a very simple calculation can be made to prove it. Consider a particle with elementary charge situated very close to a star with total charge of the same sign. In order for the particle not to be repelled by the star, the gravitational force between them has to be higher than the electromagnetic one:

$$\frac{GMm}{R^2} > \frac{Z_{\text{tot}}e^2}{R^2}, \quad (1.1)$$

where  $G$  is the gravitational constant,  $M$  is the star mass,  $m$  is the particle mass,  $R$  is the radius of the star,  $Z_{\text{tot}} e$  is the total charge of the star and  $e$  is the elementary charge. As the baryonic mass of the star ( $A m$ , where  $A$  is the number of baryons in the star) is higher than the gravitational mass ( $M$ ) we can replace it in the formula. The result is, after plugging in the numbers, that for the star not to repel the charge, the total charge per baryon inside it has to be  $Z_{\text{tot}} e/A < 10^{-36} e$ , which is practically zero.

Charge neutrality is a necessary but not sufficient assumption for stability in neutron stars, there are others. One example is chemical equilibrium, that means that the number of particles from each kind is not conserved, but they are created and annihilated through specific reactions happening at the same rate in both directions. A very important reaction is the one related to beta equilibrium that establishes how the protons and neutrons transform into each other. This kind of relation also allows

us to write the chemical equilibrium equations for all particles as a function of a small number of chemical potentials. This number is related to the number of conserved quantities in the system. In this way, we can find the fraction of each particle in each part of the star as will be shown in the following.

According to the equivalence principle of general relativity, in any gravitational space, regardless of its intensity, a free falling observer does not observe gravitational forces. The only exception being in the case of a non-uniform gravitational field like the one responsible for the tidal effects. Otherwise, the space-time is the one from special relativity, the Minkowski space. In this case it is enough to care about the microscopic physics. General relativity is only taken into account for the calculation of global properties of the star. In this case, gravity is included through the TOV equations [9, 10]. The solution of these equations correspond to the configurations in which the star is in hydrostatic equilibrium. That means that the internal pressure, coming mainly from the Fermi energy of the neutrons, balances the gravity, avoiding the collapse. But different from the classical hydrostatic equilibrium equations, the TOV equations have relativistic corrections. Finally, from this solution we have to apply the Le Chatelier principle to choose the configurations that are truly stable:

$$\frac{dp}{d\epsilon} \geq 0. \quad (1.2)$$

It requires that the derivative of the pressure with respect to the energy density has to be higher than zero, otherwise the neutron star is not stable with respect to vibration modes and collapses to black holes or dissolves into space (see chapter 3 for more details).

When rotation is included the star becomes more stable, and consequently, can be more massive. The movement also makes it more flat, which requires the metric of the star to also be a function of the polar coordinate  $\theta$  (in the TOV equations only the radial coordinate  $r$  is taken into account). Another important feature that has to be included is the dragging of the local inertial frame. It generates centrifugal forces that are not originated in interactions with other bodies, but from the rotation of the frame of reference within which observations are made. These modifications are introduced through the Hartle's approximation that solves the problem by applying perturbation theory [11]. The energy and pressure are the ones from TOV equations plus corrections

up to second order due to rotation.

In the next chapter the non-linear sigma model [12] will be introduced. This is an effective relativistic quantum model that was developed in order to describe systems of hadrons interacting via meson exchange. The main difference between this and the simplest effective model that uses meson interactions to reproduce the attractive and repulsive parts of the strong interaction (constructed by Walecka [13]) is that in our case the model was constructed from symmetry relations, allowing it to be chirally invariant. The first consequence of this invariance is that there are no bare mass terms in the lagrangian density, causing all, or most of the particles masses to come from the interactions with the medium. After constructing the model, the mean field approximation will be applied in order to obtain the equations of motion and the equation of state.

In chapter three the high asymmetry between protons and neutrons together with the charge neutrality and beta equilibrium will characterize neutron star matter. Gravity will come into play through the TOV equations in order to determine the global properties of the star. Different configurations and constituents will be analyzed and observations will be used to select which is the best option. In chapter four, the first moments of the neutron star life, when it is called proto-neutron star will be modeled with the introduction of finite temperature and high lepton number (also implying high proton fraction). These features define the stages of the star evolution and establish constraints on important properties of the cold star. These constraints will be again calculated in chapter five with the inclusion of rotational effects.

The sixth chapter will introduce quarks into the model. There will be a new effective potential calibrated in order to reproduce lattice QCD and heavy ion collision results. The improved model can be used to model matter not only at high densities but also high temperatures. The new order parameter related to deconfinement is the Polyakov loop, and together with the chiral condensate (related to the chiral symmetry restoration) it can be used to construct a phase diagram. Finally, this matter containing different degrees of freedom (depending on which phase of the diagram we are) will be used to calculate hybrid star properties.



## 2 The Nonlinear Realization of the Sigma Model

In this chapter the basic model used for all the calculations of this dissertation will be presented. It consists of a chiral  $SU(3) \times SU(3)$   $\sigma - \omega$  type model. This means that its most important feature is allowing a chirally symmetric phase. The relevant degrees of freedom are baryons that interact through mesons. The scalar mesons (as the  $\sigma$ ) represent the attractive part of the strong force while the vector mesons (as the  $\omega$ ) generate the repulsive part.

At least up to energies achieved nowadays in experiments, Quantum Chromo Dynamics is the underlying theory of the strong interaction. The degrees of freedom of this theory are quarks that interact through gluon exchange. The problem is that due to a very peculiar characteristic of the strong force, called confinement, the force between quarks does not diminish as they are separated [14, 15]. On the other hand, the interactions become weaker as the mutual distance decreases or as the exchange of momentum increases. At high temperatures or densities the interactions which confine quarks and gluons inside hadrons become weak enough to release them. This decrease of the coupling strength is called asymptotic freedom.

Nevertheless there are some possible ways to circumvent the problem. The first one is to apply perturbative techniques. At high-temperatures or chemical potentials the typical momentum exchanges become large and consequently the coupling constant of the theory become small. In the asymptotic regimes perturbative QCD (pQCD) techniques can be used [16, 17, 18]. However, for temperatures and chemical potentials near the phase transition or below, the strong coupling constant becomes large. For this reason perturbative treatments cannot be applied to neutron star matter.

The second method is to use lattice QCD [19]. In this case the space-time is represented by a crystalline lattice in which the vertices (quarks) are connected by lines (where gluons travel). Taking the limit in which the discretized lattice spacing becomes smaller, the theory becomes closer to the true continuum theory of QCD. This method can only be used to model systems with temperature higher than the

chemical potential and low density (because of the fermion sign problem - cancellation of positive and negative contributions to the partition sum that cause large fluctuations in computed averages). This approach can clearly not be used for neutron star matter. Nevertheless, we will use it to calibrate the extended chiral model (chapter 5) that can also be applied for the high temperature/low density limit. The third method is AdS/CFT (anti-de-Sitter space/conformal field theory correspondence). The idea in AdS/CFT is that there is an equivalence between a string theory defined in a warped multidimensional space and a quantum field theory without gravity defined on the conformal boundary of this space [20, 21, 22]. In this way it describes QCD in terms of a classical gravitational theory. Although this correspondence is now widely-studied, there is still no experimental evidence for the success of this approach.

The fourth method is the use of effective models, that use phenomenological constraints to construct Lagrangian densities. They normally work in a determined range of energies, but nevertheless give good qualitative and quantitative results. Between a large amount of existent effective models, it is worth mentioning chiral perturbation theory (ChPT), which is constructed by introducing every interaction of particles not excluded by symmetry and ordering them based on the number of momentum and mass powers [23]. Another very interesting effective model is the Nambu-Jona-Lasinio model (NJL). It describes a system of fermions interacting through point-like interactions. This model takes into account chiral symmetry, but if the chosen degrees of freedom are quarks (in the original publication the degrees of freedom were nucleons [24, 25]), there is no confinement.

The matter in neutron stars is considered to have low energies, except the very inner core. The inner core will be treated differently in chapter 5. In this case, the effective degrees of freedom are hadrons. In spite of that, relevant aspects of QCD as for example symmetries can and should still be taken into account.

## 2.1 Symmetries

It is known from Noether's theorem that the invariance of the Lagrangian density of a system with respect to global continuous symmetries implies corresponding conserved currents [26]. For instance a  $U(1)$  transformation is done by the multiplication of the

particle field by a global phase factor

$$\Psi(x) \rightarrow e^{i\theta}\Psi(x), \quad (2.1)$$

where  $\Psi(x) = u(x), d(x), s(x)$ . If the lagrangian is invariant under the transformation, the associated conserved charge is the baryon number

$$B = \frac{1}{3} \int d^3x \Psi(x)^\dagger \Psi(x). \quad (2.2)$$

In the same way the chiral symmetry operations, that can be separated into left-handed and right-handed projections  $SU(3)_L \times SU(3)_R$ , are

$$\Psi(x)_L \rightarrow e^{i\theta_L^a \lambda_a} \Psi(x)_L \equiv L\Psi(x)_L, \quad (2.3)$$

$$\Psi(x)_R \rightarrow e^{i\theta_R^a \lambda_a} \Psi(x)_R \equiv R\Psi(x)_R, \quad (2.4)$$

where  $\{\lambda_a\} (a = 1, \dots, 8)$  are the eight  $SU(3)$  Gell-Mann matrices. These expressions can also be rewritten as vector and axialvector transformations  $SU(3)_V \times SU(3)_A$ :

$$\Psi(x) \rightarrow e^{-i\theta_V^a \lambda_a} \Psi(x), \quad (2.5)$$

$$\Psi(x) \rightarrow e^{-i\gamma_5 \theta_A^a \lambda_a} \Psi(x), \quad (2.6)$$

where the matrix  $\gamma_5 = \begin{pmatrix} 0 & 1 \\ 1 & 0 \end{pmatrix}$  changes the orientation of the basis vectors of the group. The phase factors are related through  $\theta_V = (\theta_L + \theta_R)/2$  and  $\theta_A = (\theta_L - \theta_R)/2$ . The associated conserved quantities are the vector currents

$$V_a^\mu = \bar{\Psi} \gamma^\mu \frac{\lambda_a}{2} \Psi, \quad (2.7)$$

and the the axial currents

$$A_a^\mu = \bar{\Psi} \gamma^\mu \gamma_5 \frac{\lambda_a}{2} \Psi, \quad (2.8)$$

where  $\bar{\Psi} = \Psi^\dagger \gamma^0$  and  $\{\gamma^\mu\}$  are the Dirac matrices. When applied to the QCD vacuum, the vector charges  $Q_a^V$  leave the state invariant  $Q_a^V |0\rangle = |0\rangle$  while the axial-vector charges  $Q_a^A$  do not  $Q_a^A |0\rangle \neq |0\rangle$ . In another words, chiral symmetry is not an exact

symmetry of nature. This can easily be seen from the the absence of parity doublets, that are two states with the same mass but opposite parity (concept of mirror reflection between “left” and “right”). Examples of these are the  $\rho(770)$  and the  $a_1(1260)$  meson, the nucleon  $N(938)$  and the  $N^*(1535)$  resonance. Since the values of the current quark masses are small compared to hadronic states, the large mass splitting between the chiral partners cannot result from this contribution. Therefore, it can be concluded that the chiral symmetry is spontaneously broken, meaning that even if the Lagrangian density of the system is chirally symmetric, the ground state is not.

Every time a symmetry is spontaneously broken into a subgroup, meaning that a system that is symmetric with respect to some symmetry group goes into a vacuum state that is not symmetric, massless particles called Goldstone bosons appear in the model. They correspond to broken symmetry generators and can be thought of as excitations of the field in the symmetric “directions”. Their nature depend mostly on the nature of the symmetry. When a symmetry is not exact, i.e., if it is explicitly broken as well as spontaneously broken (as in the model defined in this chapter), the particles that appear are called pseudo-Goldstone bosons. Instead of being massless they have a very small mass. Because there are eight axial charges  $Q_\alpha^A$ , there are eight pseudo-Goldstone bosons identified with the eight lightest pseudo-scalar mesons. They are particles with spin zero but odd parity, that means that they have their sign flipped by spatial inversion.

The vacuum is populated by a condensate of scalar quark-antiquark pairs with non-vanishing expectation value. It is defined as  $\langle 0|\bar{q}q|0\rangle \equiv \langle \bar{q}q\rangle = \langle \bar{u}u\rangle + \langle \bar{d}d\rangle + \langle \bar{s}s\rangle$ . The scalar operator  $\bar{\Psi}\Psi$  can be projected onto left and right-handed parts as

$$\bar{\Psi}\Psi = (\bar{\Psi}_L + \bar{\Psi}_R)(\Psi_L + \Psi_R) = \bar{\Psi}_L\Psi_R + \bar{\Psi}_R\Psi_L, \quad (2.9)$$

where the terms  $\bar{\Psi}_L\Psi_L$  and  $\bar{\Psi}_R\Psi_R$  vanish. This can be verified with the definition of the left and right-handed projection:

$$\Psi_L = \frac{(1 - \gamma_5)}{2}\Psi \quad \text{and} \quad \Psi_R = \frac{(1 + \gamma_5)}{2}\Psi, \quad (2.10)$$



and their adjoints

$$\bar{\Psi}_L = \Psi^\dagger \frac{(1 - \gamma_5)}{2} \gamma_0 = \bar{\Psi} \frac{(1 + \gamma_5)}{2} \quad \text{and} \quad \bar{\Psi}_R = \Psi^\dagger \frac{(1 + \gamma_5)}{2} \gamma_0 = \bar{\Psi} \frac{(1 - \gamma_5)}{2}, \quad (2.11)$$

where it was used that  $\{\gamma_0, \gamma_5\} = 0$ . It is easy to see that terms containing the adjoints of the field followed by the field are equal to zero using  $\gamma_5^2 = I$ .

The terms of Eq. 2.9 mix left- and right-handed quarks and therefore break chiral symmetry. For this reason the condensate plays the role of the order parameter for the chiral symmetry restoration. If it has non zero value, the chiral symmetry is broken.

## 2.2 Anomalies

In classical physics an anomaly is the failure of a symmetry to be restored in the limit in which the order parameter goes to zero. In quantum physics an anomaly is the failure of a classical symmetry. The first one analyzed is the axial  $U(1)$  anomaly. If the system is invariant under the transformation

$$\Psi(x) \rightarrow e^{i\theta\gamma_5}\Psi(x), \quad (2.12)$$

there is an associated ninth conserved current

$$A_0^\mu = \bar{\Psi}\gamma^\mu\gamma_5\Psi, \quad (2.13)$$

whose divergence is equal to zero  $\partial_\mu A_0^\mu = 0$ . However, in quantum field theory this quantity does not vanish, being instead proportional to the gluon fields  $\partial_\mu A_0^\mu = \frac{\alpha_s}{4\pi} N_f G_{\mu\nu} G^{\mu\nu}$ , with  $\alpha_s$  being the QCD running coupling strength and  $N_f$  the number of flavors. Because of the axial  $U(1)$  anomaly, the symmetry from QCD that was  $U(3)_L \times U(3)_R$  or  $SU(3)_L \times SU(3)_R \times U(1)_V \times U(1)_A$  is spontaneously broken to  $SU(3)_V \times U(1)_V \times U(1)_A$  and then reduced to  $SU(3)_V \times U(1)_V$ .

Another important anomaly from QCD is the trace anomaly. At the classical level the system is invariant under the transformations

$$\Psi(x) \rightarrow \lambda^\Delta \Psi(\lambda x), \quad (2.14)$$

where  $\lambda$  is arbitrary and  $\Delta = 2/3$  for spin 1/2 fields. At the limit of vanishing quark masses, there are no dimensionful parameters in the QCD Lagrangian and the classical behavior is recovered. The associated conserved dilaton current is

$$J_{\text{scale}}^\mu = \chi_\nu T^{\mu\nu}, \quad (2.15)$$

whose divergence together with the trace of the energy momentum tensor  $T^{\mu\nu}$ , should be equal to zero:  $\partial_\mu J_{\text{scale}}^\mu = T_\nu^\nu = 0$ . However, in quantum field theory it does not vanish, but is proportional to the gluon fields. This happens because of the introduction of a scale, meaning that to fully specify QCD, not only the Lagrangian, but the scale parameter also has to be specified. In this case the energy momentum tensor becomes

$$T_\mu^\mu = \frac{\beta_{\text{QCD}}}{2g} G_{\mu\nu} G^{\mu\nu}, \quad (2.16)$$

with  $\beta_{\text{QCD}} = 11 - 2N_f/3$  and  $g$  is a coupling constant. Therefore, the quantum theory is not scale invariant and the dilaton currents are not conserved. In another words, the strength of the particle interactions (coupling parameters) do depend on the energy-scale involved. To mimic this behavior in the effective theory, we introduce a scalar field  $\chi$ . The lagrangian for this field is introduced in the following and yields a trace of its energy-momentum tensor as

$$T_\mu^\mu = \chi^4. \quad (2.17)$$

Thus in mean field approximation  $\chi^4$  corresponds to the gluon condensate  $\langle G_{\mu\nu} G^{\mu\nu} \rangle$  with a vacuum value of  $\chi_0^4$ .

## 2.3 Construction of the Model

The hadronic degrees of freedom of the model are the lowest  $SU(3)$  multiplets, the baryon octet and decuplet, the scalar, pseudo-scalar and vector meson nonets. It is important to remember that although a simple way to describe hadronic matter properties is to use hadrons as degrees of freedom, the general properties of the underlying theory still have to be taken into account. For example the quark condensate strongly determines the properties of hadrons. At high temperatures/densities chiral symmetry is expected to be restored and this should be visible in the hadron masses.

It is already known that bare mass terms like in Eq. 2.9 mix left- and right-handed fields and therefore break chiral symmetry. It is possible though to construct effective masses for the baryons as a function of chirally invariant terms. For example the term  $(\bar{\Psi}\Psi)^2 + (\bar{\Psi}i\gamma_5\Psi)^2$  that can be rewritten as  $\bar{\Psi}(\sigma + i\gamma_5\pi)\Psi$  with the definition of  $\sigma = \langle \bar{\Psi}\Psi \rangle$  and  $\pi = \langle \bar{\Psi}i\gamma_5\Psi \rangle$  is chiral invariant at the limit of vanishing  $\sigma$  and  $\pi$ . Terms like powers of  $\sigma^2 + \pi^2$  are also invariants. These are the basis of the widely used linear sigma model [27, 28]. Although this kind of model can reproduce hadronic masses and nuclear matter reasonably well, it has been shown that the hyperon potentials come out too large [27]. In this case the strange scalar meson  $\zeta$  ( $\sigma^*$ ) couples to the non-strange scalar field  $\sigma$  ( $f_0$ ) and changes considerably in the nuclear medium even for zero strangeness.

The nonlinear realization of chiral symmetry was introduced to generate a pseudovector  $\pi - N$  coupling to allow heavy degrees of freedom to transform in a different representation, such that they transform equally under left and right chiral transformations. The resulting advantages are many:

- the pseudoscalar mesons exhibit a pseudovector coupling to the baryons in agreement with the experimental finding of a vanishing  $\pi - N$ -scattering length
- chiral invariance for heavy particles is ensured if their coupling is invariant under local  $SU(3)_V$  transformations (allowing couplings between baryons and meson octets)
- baryon masses can be fitted to experimental data without explicit symmetry breaking terms
- a connection to the phenomenological Walecka model exists [12]
- the masses of the pseudoscalar mesons do not become imaginary at high densities.

The idea of the model was introduced by Weinberg [29] for the  $SU(2)_L \times SU(2)_R$  and extended to higher dimensions [30, 31]. In the following the group  $SU(3)_L \times SU(3)_R$  with the subgroup  $SU(3)_V$  is considered. An element  $g$  of  $SU(3)_L \times SU(3)_R$  can be decomposed into

$$g = e^{i\sum \zeta_a Q_a^5} e^{i\sum \theta_b Q_b} \equiv \mathbf{u}[\zeta]\mathbf{h}[\theta], \quad (2.18)$$

where  $\zeta$  and  $\theta$  are parameters of the transformations and are generally space-time dependent,  $Q$  and  $Q^5$ , that are respective the vector and axial charges, are the generators of the group  $SU(3)_L \times SU(3)_R$  and  $h$  is an element of  $SU(3)_V$ . Assuming global invariance under  $SU(3)_L \times SU(3)_R$  transformation,  $g$  becomes

$$g = e^{i\sum \alpha_L^a \lambda_{La}} e^{i\sum \alpha_R^b \lambda_{Rb}} \equiv L(\alpha_L)R(\alpha_R), \quad (2.19)$$

where  $\alpha_L$  and  $\alpha_R$  are space-time independent parameters and  $\lambda_L = \lambda(1 - \gamma_5)/2$  and  $\lambda_R = \lambda(1 + \gamma_5)/2$  are Gell-Mann matrices acting in the left and right handed space, respectively. The product  $gu$  is still an element of  $SU(3)_L \times SU(3)_R$  and can be written as

$$gu = e^{i\sum \zeta'_a Q_a^5} e^{i\sum \theta'_b Q_b}, \quad (2.20)$$

where  $\zeta'$  and  $\theta'$  depend on  $g$  and  $\zeta_a$ . If a linear representation of the subgroup  $SU(3)_V$  is  $q \rightarrow D(h)q$ , a nonlinear representation of the group  $SU(3)_L \times SU(3)_R$  would be  $q \rightarrow e^{i\sum \theta'_b Q_b} q$ , with  $\zeta \rightarrow \zeta'$ . Associating the parameters of the axial charges  $\zeta$  with the pseudoscalar mesons [32] one has

$$u = e^{i\pi^a Q_a^5}. \quad (2.21)$$

Because the pseudoscalar mesons are the parameters of the symmetry transformation, they will only appear if the symmetry is explicitly broken or in terms with derivatives of the fields.

Therefore to build a model with hadronic degrees of freedom, their composition in terms of quarks has to be determined [27]. The transformation properties of the hadrons in the nonlinear representation can be derived from the relation between the quarks in the linear ( $q$ ) and nonlinear ( $\tilde{q}$ ) representation. The quarks of the nonlinear representation transform with the vector subgroup  $SU(3)_V$  in accord with Eq. 2.18 setting  $h \rightarrow 1$ . Splitting them into left- and right-handed parts, they can be written as

$$q_L = u\tilde{q}_L \quad \text{and} \quad q_R = u^\dagger\tilde{q}_R, \quad (2.22)$$

where these equations are connected by parity. The transformation properties of the

new quarks are found by considering how the old quarks transform

$$q' = Lq_L + Rq_R = Lu\tilde{q}_L + Ru^\dagger\tilde{q}_R. \quad (2.23)$$

According to Eq. 2.20,

$$Lu = u'h \quad \text{and} \quad Ru^\dagger = u'^\dagger h, \quad (2.24)$$

with  $g = L$ . By inserting these expressions in Eq. 2.23 and using Eq. 2.22, one sees that  $\tilde{q}$  transforms as

$$\tilde{q}'_L = h\tilde{q}_L \quad \text{and} \quad \tilde{q}'_R = h\tilde{q}_R. \quad (2.25)$$

According to Eq. 2.20, in general the vector transformation is a local nonlinear function depending on pseudoscalar mesons  $h = h[g, \pi_a]$ . Following Eq. 2.24, the pseudoscalar mesons transform nonlinearly as

$$u' = Lu h^\dagger = huR^\dagger \quad \text{and} \quad u'^\dagger = hu^\dagger L^\dagger = Ru^\dagger h^\dagger. \quad (2.26)$$

In contrast with the linear realization of chiral symmetry, there is no distinction between the left and the right space. The various octets transform accordingly

$$X' = hXh^\dagger, \quad V'_\mu = hV_\mu h^\dagger, \quad \mathcal{A}'_\mu = h\mathcal{A}_\mu h^\dagger, \quad B' = hBh^\dagger, \quad (2.27)$$

where  $X$  is the scalar matrix,  $V_\mu = l_\mu + r_\mu$  the vector,  $\mathcal{A}_\mu = l_\mu - r_\mu$  the axial vector and  $B$  the baryon.  $l_\mu$  and  $r_\mu$  are the left and right handed parts of the spin-1 mesons in the linear representation. The hadronic fields that transform nonlinearly can be obtained from the ones that transform linearly (described in [27]) by multiplying them by  $u[\pi]$  and its conjugate

$$X = \frac{1}{2}(u^\dagger M u^\dagger + u M^\dagger u), \quad Y = \frac{1}{2}(u^\dagger M u^\dagger - u M^\dagger u), \quad (2.28)$$

$$l_\mu = u^\dagger \tilde{l}_\mu u, \quad r_\mu = u \tilde{r}_\mu u^\dagger, \quad (2.29)$$

$$B_L = u^\dagger \Psi_L u, \quad B_R = u \Psi_R u^\dagger, \quad (2.30)$$

where  $Y$  is the pseudoscalar matrix and  $M = \Sigma + i\Pi$  and its conjugate contain the

nonets of the linearly transforming scalar  $\Sigma$  and pseudoscalar  $\Pi$ .  $\Psi_L$  and  $\Psi_R$  are the left and right handed parts of the baryons in the linear representation.

## 2.4 The Nonlinear Realization of the Sigma Model

The Lagrangian density of the nonlinear sigma model reads

$$\mathcal{L} = \mathcal{L}_{\text{Kin}} + \mathcal{L}_{\text{int}} + \mathcal{L}_{\text{scal}} + \mathcal{L}_{\text{vec}} + \mathcal{L}_{\text{SB}}, \quad (2.31)$$

where  $\mathcal{L}_{\text{Kin}}$  is the kinetic energy term,  $\mathcal{L}_{\text{int}}$  is the interaction term between baryons and mesons,  $\mathcal{L}_{\text{scal}}$  is the self-interaction term for the spin-0 mesons,  $\mathcal{L}_{\text{vec}}$  is the self-interaction term for the spin-1 mesons and  $\mathcal{L}_{\text{SB}}$  is the explicit symmetry breaking term. In the following each of these parts will be explained.

### 2.4.1 Kinetic energy term

The kinetic term is given as in [12]

$$\begin{aligned} \mathcal{L}_{\text{Kin}} = & i\text{Tr}(\bar{B}\gamma_\mu D^\mu B) + \frac{1}{2}\text{Tr}(D_\mu X D^\mu X) + \text{Tr}(u_\mu X u^\mu X + X u_\mu u^\mu X) \\ & + \frac{1}{2}\text{Tr}(D_\mu Y D^\mu Y) + \frac{1}{2}\text{Tr}(D_\mu \chi D^\mu \chi) - \frac{1}{4}\text{Tr}(\tilde{V}_{\mu\nu} \tilde{V}^{\mu\nu}) - \frac{1}{4}\text{Tr}(\tilde{A}_{\mu\nu} \tilde{A}^{\mu\nu}), \end{aligned} \quad (2.32)$$

where the first term is the Dirac kinetic term for baryon octet, the second is the Klein-Gordon kinetic term for the scalar meson multiplet, the third comes from an interaction between the scalar and the pseudoscalar mesons and also contains the kinetic term for the pseudoscalar meson octet, the fourth term is the Klein-Gordon kinetic term for the pseudoscalar meson singlet, the fifth is the Klein-Gordon kinetic term for the scalar-isoscalar glueball field, the sixth is the Proca kinetic term for the vector meson multiplet, the seventh term is the Proca kinetic term for the axial vector meson multiplet. The axial vector  $u_\mu$  is defined as  $u_\mu = -\frac{i}{2}[u^\dagger \partial_\mu u - u \partial_\mu u^\dagger]$ , the vector field tensor is  $\tilde{V}_{\mu\nu} = \partial^\mu \tilde{V}^\nu - \partial^\nu \tilde{V}^\mu$  and the axial-vector field tensor is  $\tilde{A}_{\mu\nu} = \partial_\mu \tilde{A}_\nu - \partial_\nu \tilde{A}_\mu$ . The covariant derivative is  $D_\mu = \partial_\mu + i[\Gamma_\mu, B]$  (for the baryons), with  $\Gamma_\mu = -\frac{i}{2}[u^\dagger \partial_\mu u - u \partial_\mu u^\dagger]$  assuring chiral invariance.

### 2.4.2 Interaction term between baryons and mesons

The structure of the baryon-meson interaction terms is the same for all mesons except for the difference in Lorentz space. It reads

$$\mathcal{L}_{\text{int}} = -\sqrt{2}g_8^W \left\{ \alpha_W [\bar{B}\mathcal{O}BW]_{AS} + (1 - \alpha_W) [\bar{B}\mathcal{O}BW]_S \right\} - g_1^W \frac{1}{\sqrt{3}} \text{Tr}(\bar{B}\mathcal{O}B) \text{Tr}(W), \quad (2.33)$$

where the antisymmetric coupling is  $[\bar{B}\mathcal{O}BW]_{AS} = \text{Tr}(\bar{B}\mathcal{O}WB - \bar{B}\mathcal{O}BW)$  and the symmetric one is  $[\bar{B}\mathcal{O}BW]_S = \text{Tr}(\bar{B}\mathcal{O}WB + \bar{B}\mathcal{O}BW) - \frac{2}{3} \text{Tr}(\bar{B}\mathcal{O}B) \text{Tr}(W)$ . The matrices  $\mathcal{O}$  and  $W$  depend on the interaction considered.  $\mathcal{O} = 1$  and  $W = X$  stand for the interaction between the baryons and the scalar mesons,  $\mathcal{O} = \gamma_\mu \gamma_5$  and  $W = u_\mu$  for the interaction between the baryons and the pseudoscalar mesons,  $\mathcal{O} = \gamma_\mu$  and  $W = \tilde{V}_\mu$  for the vector part of the interaction between the baryons and the vector mesons,  $\mathcal{O} = \sigma^{\mu\nu}$  and  $W = \tilde{V}_{\mu\nu}$  for the tensor part of the interaction between the baryons and the vector mesons and  $\mathcal{O} = \gamma_\mu \gamma_5$  and  $W = \tilde{A}_\mu$  for the interaction between the baryons and the axial-vector mesons.

When heavier degrees of freedom are included in the model, e.g. spin 3/2 resonances ( $D_\mu$ ), a similar coupling can be defined and added to the Lagrangian

$$\mathcal{L}_{\text{int}} = \mathcal{L}_{\text{int}} - \sqrt{2}g_{D_8}^W [\bar{D}^\mu \mathcal{O} D_\mu W] - g_{D_1}^W [\bar{D}^\mu \mathcal{O} D_\mu] \text{Tr}(W), \quad (2.34)$$

where  $[\bar{D}^\mu \mathcal{O} D_\mu W]$  and  $[\bar{D}^\mu \mathcal{O} D_\mu]$  are obtained from the coupling of  $D_\mu$  with the mesonic matrices [33].

#### Interaction with the scalar mesons

Effective masses for the baryons can be calculated from the interaction part of the Lagrangian density. Replacing the scalar matrix  $X$  (ignoring the meson  $\delta$  for now) and the baryonic matrix  $B$  (and its adjunct) from the appendix in Eq. 2.33 and equating the whole expression to minus the effective masses of the baryons, we get

$$M_N^* = g_1^X \frac{1}{\sqrt{3}} (\sqrt{2}\sigma + \zeta) - g_8^X \frac{1}{3} (4\alpha_X - 1) (\sqrt{2}\zeta - \sigma), \quad (2.35)$$

$$M_{\Lambda}^* = g_1^X \frac{1}{\sqrt{3}} (\sqrt{2}\sigma + \zeta) - g_8^X \frac{1}{3} (\alpha_X - 1) (\sqrt{2}\zeta - \sigma), \quad (2.36)$$

$$M_{\Sigma}^* = g_1^X \frac{1}{\sqrt{3}} (\sqrt{2}\sigma + \zeta) + g_8^X \frac{1}{3} (\alpha_X - 1) (\sqrt{2}\zeta - \sigma), \quad (2.37)$$

$$M_{\Xi}^* = g_1^X \frac{1}{\sqrt{3}} (\sqrt{2}\sigma + \zeta) + g_8^X \frac{1}{3} (2\alpha_X - 1) (\sqrt{2}\zeta - \sigma), \quad (2.38)$$

where,  $\sigma \sim \langle \bar{u}u + \bar{d}d \rangle$  and  $\zeta \sim \langle \bar{s}s \rangle$ . Using, instead of the matrix  $X$  its vacuum expectation value  $\langle X \rangle$ , the effective masses  $M^*$  become the vacuum masses  $M$  for the baryons. In this way, we can use their measured vacuum masses to calculate the coupling constants  $g_1^X$ ,  $g_8^X$  and  $\alpha_X$ . It is important to note that the nucleon effective mass  $M_N^*$  depends on the strange condensate  $\zeta$ . A case in which this does not happen can be constructed, though in this case explicit symmetry breaking terms have to be included to fit the vacuum masses [12]. It is important to note that if  $\zeta = \sigma/\sqrt{2}$  the masses of the baryons are degenerate and the vacuum is  $SU(3)_V$  invariant.

For the baryon decuplet the procedure is the same. The members are treated as spin 1/2 particles with spin 3/2 degeneracy. Using the scalar matrix  $X$  and the baryonic decuplet matrix  $D_{\mu}$ , that can be constructed using the quark representation in the same way as  $B$ , and equating the whole expression to negative of the effective masses of the baryons, we get

$$M_{\Delta}^* = g_D^X [(3 - \alpha_{DX})\sigma + \alpha_{DX}\sqrt{2}\zeta], \quad (2.39)$$

$$M_{\Sigma^*}^* = g_D^X [2\sigma + \sqrt{2}\zeta], \quad (2.40)$$

$$M_{\Xi^*}^* = g_D^X [(1 + \alpha_{DX})\sigma + (2 - \alpha_{DX})\sqrt{2}\zeta], \quad (2.41)$$

$$M_{\Omega}^* = g_D^X [2\alpha_{DX}\sigma + (3 - 2\alpha_{DX})\sqrt{2}\zeta], \quad (2.42)$$



where the new parameter  $g_D^X$  relates to the old ones through  $g_{D1}^X = \sqrt{90}g_D^X$  and  $g_{D8}^X = -\sqrt{120}(1 - \alpha_{DX})g_D^X$ . They can now be calculated in order to reproduce the measured vacuum masses of the decuplet. As in the case of the nucleon, the mass of the  $\Delta$  also depends on the strange condensate  $\zeta$ .

### Interaction with the vector mesons

The interaction terms with vector mesons are similar to the one with scalar mesons. The only difference is that the symmetric coupling should be small and in this case only the antisymmetric part will be used ( $\alpha_V = 1$ ). This statement is in agreement with the universality principle [34] and the vector meson dominance model. We set  $g_1^V = \sqrt{6}g_8^V$  so the strange meson  $\phi$  does not couple to the nucleons. Replacing the vector matrix  $\tilde{V}_\mu$  from the appendix in Eq. 2.33 we obtain the following relations

$$g_{N\omega} = 3g_8^V, \quad g_{N\phi} = 0, \quad g_{N\rho} = g_8^V = \frac{1}{3}g_{N\omega}, \quad (2.43)$$

$$g_{\Lambda\omega} = 2g_8^V = \frac{2}{3}g_{N\omega}, \quad g_{\Lambda\phi} = -\sqrt{2}g_8^V = -\frac{\sqrt{2}}{3}g_{N\omega}, \quad g_{\Lambda\rho} = 0, \quad (2.44)$$

$$g_{\Sigma\omega} = 2g_8^V = \frac{2}{3}g_{N\omega}, \quad g_{\Sigma\phi} = -\sqrt{2}g_8^V = -\frac{\sqrt{2}}{3}g_{N\omega}, \quad g_{\Sigma\rho} = 2g_8^V = \frac{2}{3}g_{N\omega}, \quad (2.45)$$

$$g_{\Xi\omega} = g_8^V = \frac{1}{3}g_{N\omega}, \quad g_{\Xi\phi} = -2\sqrt{2}g_8^V = -\frac{2\sqrt{2}}{3}g_{N\omega}, \quad g_{\Xi\rho} = g_8^V = \frac{1}{3}g_{N\omega}. \quad (2.46)$$

To couple the baryon decuplet, the procedure is the same as for the octet but the matrix replaced in Eq. 2.33 is  $D_\mu$  and  $\alpha_{DV} = 0$  in order for the strange meson  $\phi$  not to couple to  $\Delta$ .

$$g_{\Delta\omega} = 3g_8^V, \quad g_{\Delta\phi} = 0, \quad g_{\Delta\rho} = 3g_8^V = g_{\Delta\omega}, \quad (2.47)$$

$$g_{\Sigma^*\omega} = 2g_8^V = \frac{2}{3}g_{\Delta\omega}, \quad g_{\Sigma^*\phi} = -\sqrt{2}g_8^V = -\frac{\sqrt{2}}{3}g_{\Delta\omega}, \quad g_{\Sigma^*\rho} = 2g_8^V = \frac{2}{3}g_{\Delta\omega}, \quad (2.48)$$

$$g_{\Xi^*\omega} = g_8^V = \frac{1}{3}g_{\Delta\omega}, \quad g_{\Xi^*\phi} = -2\sqrt{2}g_8^V = -\frac{2\sqrt{2}}{3}g_{\Delta\omega}, \quad g_{\Xi^*\rho} = g_8^V = \frac{1}{3}g_{\Delta\omega}, \quad (2.49)$$

$$g_{\Omega\omega} = 0, \quad g_{\Omega\phi} = -3\sqrt{2}g_8^V = -\sqrt{2}g_{\Delta\omega}, \quad g_{\Omega\rho} = 0. \quad (2.50)$$

According to these expressions, as soon as  $g_8^V$  or  $g_{N\omega}$  is specified, all the vector coupling constants are fixed.

### 2.4.3 Self interaction term for the spin-0 mesons

The couplings of the scalar mesons are governed by the  $SU(3)_V$  symmetry. The only possible invariants are

$$I_1 = \text{Tr}(X), \quad I_2 = \text{Tr}(X)^2, \quad I_3 = \det(X). \quad (2.51)$$

All other powers of  $\text{Tr}(X)$  can be expressed as a function of these 3 invariants. For example,

$$I_4 = \text{Tr}(X)^4 = I_1 I_{3m} + \frac{1}{2}[I_2 - (I_1)^2]I_2 + I_3 I_1, \quad (2.52)$$

with

$$I_{3m} = \text{Tr}(X)^3 = I_1 I_2 + \frac{1}{2}[I_2 - (I_1)^2]I_1 + I_3. \quad (2.53)$$

Different possible invariants can be constructed from these terms. We follow the one suggested by [12] used in the linear  $\sigma$  model

$$\mathcal{L}_{\text{scal}} = -\frac{1}{2}k_0\chi^2 I_2 + k_1(I_2)^2 + k_2 I_4 + 2k_3\chi I_3, \quad (2.54)$$

where  $\chi$  represents the scalar gluon field. It allows one to have a scale invariant Lagrangian density when we multiply all terms by powers of the glueball field in such a way that the terms end up having dimension  $[\text{mass}]^4$  [35]. Introducing a scale breaking term, the Lagrangian becomes

$$\mathcal{L}_{\text{scal}} = \mathcal{L}_{\text{scal}} - \frac{1}{4}\chi^4 \ln \frac{\chi^4}{\chi_0^4} + \frac{\epsilon}{3}\chi^4 \ln \frac{I_3}{\det \langle X \rangle_0} - k_4\chi^4, \quad (2.55)$$

where the value  $\epsilon = 6/33$  originates from the quark contribution to the QCD beta function  $\beta_{\text{QCD}}$ . The first term in the Lagrangian above describes the contribution from the gluons, the second the contribution from the quarks and the third term ensures that the finite vacuum expectation value  $\chi_0 = 401.93$  MeV, which corresponds to the gluon condensate in the QCD vacuum, is reproduced. The parameters  $k_0, k_1, k_2, k_3$  and  $k_4$  are calculated in order to ensure correct vacuum expectation values for  $\sigma, \zeta,$  and  $\chi$  field equations and to reproduce  $\sigma, \eta,$  and  $\eta'$  vacuum masses.

In this work the value of the field  $\chi$  is kept fixed to its vacuum value. This is done based on the fact that the glueball field does not couple strongly to the baryonic degrees of freedom, remaining "frozen" below the chiral transition. A full study of its behavior and the consequences for scale symmetry restoration can be found in [36].

#### 2.4.4 Self interaction term for the spin-1 mesons

This part of the Lagrangian density contains the mass terms of the vector mesons together with higher order of vector meson self-interactions. It reads

$$\mathcal{L}_{\text{vec}} = \frac{1}{2}m_V^2 \frac{\chi^2}{\chi_0^2} \text{Tr}(\tilde{V}_\mu \tilde{V}^\mu) + \frac{1}{4}c_1 \text{Tr}(\tilde{V}_\mu \tilde{V}^\mu X_0) + \frac{1}{12}c_2 [\text{Tr}(\tilde{V}_{\mu\nu})]^2, \quad (2.56)$$

where the last two terms were added in order to split the meson masses [37, 38, 39, 40]. The problem is that these two terms generate undesired extra contributions to the kinetic energy. To solve this problem the meson fields are renormalized (see [27] for more details) giving

$$\mathcal{L}_{\text{vec}} = \frac{1}{2} \frac{\chi^2}{\chi_0^2} (m_\omega^2 \omega^2 + m_\phi^2 \phi^2 + m_\rho^2 \rho^2). \quad (2.57)$$

The vector meson self-interaction can be written in terms of different possible invariants. Including them in the Lagrangian, it becomes:

$$\mathcal{L}_{\text{vec } 1} = \mathcal{L}_{\text{vec}} - \frac{g_4}{4} [\text{Tr}(\tilde{V}_\mu)]^4, \quad (2.58)$$

$$\mathcal{L}_{\text{vec } 2} = \mathcal{L}_{\text{vec}} - g_4 [\text{Tr}(\tilde{V}_\mu \tilde{V}^\mu)]^2, \quad (2.59)$$

$$\mathcal{L}_{\text{vec } 3} = \mathcal{L}_{\text{vec}} - 2g_4 \text{Tr}[(\tilde{V}_\mu \tilde{V}^\mu)^2]. \quad (2.60)$$

These three different options will be discussed in the next chapter due to their importance for neutron star properties.

#### 2.4.5 Explicit symmetry breaking term

In the presence of spontaneously broken continuous symmetry, new types of massless excitations appear. They are called ‘‘Goldstone modes’’ and give rise to large fluctuation effects. In order to eliminate them, explicitly symmetry breaking terms have to be introduced. Additionally, it gives rise to mass terms for the pseudoscalar mesons. Using the same expression as from the linear  $\sigma$  model [12]

$$\mathcal{L}_{\text{SB}} = \text{Tr} A_p \left( \mathbf{u}(X + iY)\mathbf{u} + \mathbf{U}^\dagger(X - iY)\mathbf{u}^\dagger \right), \quad (2.61)$$

where  $A_p = \text{diag}(m_\pi^2 f_\pi, m_\pi^2 f_\pi, 2m_k^2 f_k - m_\pi^2 f_\pi) / \sqrt{2}$ ,  $m_\pi = 139$  MeV and  $m_k = 498$  MeV. Using  $f_\pi = 93.3$  MeV and  $f_k = 122$  MeV we obtain  $\sigma_0 = 93.3$  MeV and  $\zeta_0 = 106.56$  MeV.

Because of the explicit symmetry breaking mechanism, an additional term for the hyperon-scalar meson interaction can be introduced

$$\mathcal{L}_{\text{hyp}} = m_3 \text{Tr}(\bar{\Psi}\Psi + \bar{\Psi}[\Psi, S]) \text{Tr}(X - X_0), \quad (2.62)$$

where  $X_0$  is the scalar meson matrix from the appendix with the mesons having their vacuum values and  $S_b^a = -[\sqrt{3}(\lambda_8)_b^a - \delta_b^a] / 3$  with  $\lambda$ 's being the usual Gell-Mann

matrices. This extra term allows one to fit the hyperon potentials to the experimental values.

## 2.5 Mean Field Theory Approximation

In this approach, first introduced for this type of system in [41], the mesons are treated as classical fields, i.e., they are replaced by their expectation values, which are classical fields. Furthermore, if rotational invariance holds, the expectation value of the three-vector part of the vector mesons vanishes. The Lagrangian density Eq. 2.31 becomes

$$\mathcal{L}_{\text{MFT}} = \mathcal{L}_{\text{Kin}} + \mathcal{L}_{\text{int}} + \mathcal{L}_{\text{scal}} + \mathcal{L}_{\text{vec}} + \mathcal{L}_{\text{SB}}, \quad (2.63)$$

where besides the kinetic energy term for baryons and leptons, the other terms are:

$$\mathcal{L}_{\text{int}} = \sum_i \bar{\psi}_i [g_{i\omega}\gamma_0\omega + g_{i\phi}\gamma_0\phi + g_{i\rho}\gamma_0\tau_3\rho + m_i^*]\psi_i, \quad (2.64)$$

$$\mathcal{L}_{\text{vec}} = -\frac{1}{2}(m_\omega^2\omega^2 + m_\rho^2\rho^2 + m_\phi^2\phi^2)\frac{\chi^2}{\chi_0^2} + \mathcal{L}_{\text{vec},4}, \quad (2.65)$$

$$\begin{aligned} \mathcal{L}_{\text{scal}} = & \frac{1}{2}k_0\chi^2(\sigma^2 + \zeta^2 + \delta^2) - k_1(\sigma^2 + \zeta^2 + \delta^2)^2 \\ & - k_2\left(\frac{\sigma^4}{2} + \frac{\delta^4}{2} + 3\sigma^2\delta^2 + \zeta^4\right) - k_3\chi(\sigma^2 - \delta^2)\zeta \\ & + k_4\chi^4 + \frac{1}{4}\chi^4 \ln \frac{\chi^4}{\chi_0^4} - \epsilon \chi^4 \ln \frac{(\sigma^2 - \delta^2)\zeta}{\sigma_0^2\zeta_0}, \end{aligned} \quad (2.66)$$

$$\mathcal{L}_{\text{SB}} = \left(\frac{\chi}{\chi_0}\right)^2 \left[ m_\pi^2 f_\pi \sigma + \left( \sqrt{2} m_k^2 f_k - \frac{1}{\sqrt{2}} m_\pi^2 f_\pi \right) \zeta \right]. \quad (2.67)$$

The scalar-isovector meson  $\delta(\alpha_0)$  is introduced as it relates (as the  $\rho$  meson) to the high isospin asymmetry present in neutron stars and  $\tau_3$  is the isospin projection of the baryonic charge state. The baryon masses are generated by the scalar fields except for a small explicit mass term equal to  $\delta m = 150$  MeV for the nucleons,  $\delta m = 376, 58$  MeV for the hyperons and  $\delta m = 0$  MeV for the baryon decuplet. These modifications allow one to fit better star observations. The effective masses decrease at high densities with

decreasing scalar fields as the chiral symmetry is partially restored. At low densities they reproduce the experimentally known baryon masses:

$$m_i^* = g_{i\sigma}\sigma + g_{i\delta}\tau_3\delta + g_{i\zeta}\zeta + \delta m. \quad (2.68)$$

The hyperon-scalar meson interaction also generates a contribution to the effective mass of the hyperons

$$m_3^* = m_3[\sqrt{2}(\sigma - \sigma_0) + (\zeta - \zeta_0)], \quad (2.69)$$

which is added to Eq. 2.68. The terms that depend on the scalar mesons change the coupling constants of the hyperons. The terms that depend on the vacuum values of the scalar mesons are included in the bare mass term for the hyperons.

The coupling constants used to calculate neutron star properties are:  $g_{N\omega} = 11.9$ ,  $g_{N\phi} = 0$ ,  $g_{N\rho} = 4.03$ ,  $g_{N\sigma} = -9.83$ ,  $g_{N\delta} = -2.34$ ,  $g_{N\zeta} = 1.22$ ,  $k_0 = 2.37$ ,  $k_1 = 1.40$ ,  $k_2 = -5.55$ ,  $k_3 = -2.65$ ,  $k_4 = -0.23$ ,  $\epsilon = 0.06$ ,  $g_4 = 38.9$ . They allow the model to reproduce nuclear saturation properties (density  $\rho_B = 0.15 \text{ fm}^{-3}$ , binding energy per nucleon  $B/A = -16.00 \text{ MeV}$ , nucleon effective mass  $M_N^* = 0.67 M_N$ , compressibility  $K = 297.32 \text{ MeV}$ ), asymmetry energy ( $E_{\text{sym}} = 32.50 \text{ MeV}$ ), and reasonable values for the hyperon potentials ( $U_\Lambda = -29.41 \text{ MeV}$ ,  $U_\Sigma = 20.39 \text{ MeV}$ ,  $U_\Xi = -10.09 \text{ MeV}$ ).

The equations of motion for the particle fields are obtained applying the Euler-Lagrange equations to the Lagrangian density. They are

$$\begin{aligned} \sigma : \quad & g_{i\sigma}\rho_{Si} + k_0\chi^2\sigma - 4k_1(\sigma^2 + \zeta^2 + \delta^2)\sigma - 2k_2(\sigma^2 + 3\delta^2)\sigma \\ & - 2k_3\chi\sigma\zeta - 2\epsilon\frac{\chi^4\sigma}{\sigma^2 - \delta^2} + \left(\frac{\chi}{\chi_0}\right)^2 m_\pi^2 f_\pi = 0, \end{aligned} \quad (2.70)$$

$$\begin{aligned} \delta : \quad & g_{i\delta}\tau_3\rho_{Si} + k_0\chi^2\delta - 4k_1(\sigma^2 + \zeta^2 + \delta^2)\delta - 2k_2(3\sigma^2 + \delta^2)\delta \\ & + 2k_3\chi\zeta\delta + 2\epsilon\frac{\chi^4\delta}{\sigma^2 - \delta^2} = 0, \end{aligned} \quad (2.71)$$

$$\begin{aligned} \zeta: \quad & g_{i\zeta}\rho_{Si} + k_0\chi^2\zeta - 4k_1(\sigma^2 + \zeta^2 + \delta^2)\zeta - 4k_2\zeta^3 \\ & - k_3\chi(\sigma^2 - \delta^2) - \epsilon\frac{\chi^4}{\zeta} + \left(\frac{\chi}{\chi_0}\right)^2 \left(\sqrt{2}m_k^2 f_k - \frac{1}{\sqrt{2}}m_\pi^2 f_\pi\right) = 0, \end{aligned} \quad (2.72)$$

$$\omega: \quad \sum_i g_{i\omega}\rho_{Bi} - m_\omega^2 \left(\frac{\chi}{\chi_0}\right)^2 \omega + \frac{\partial\mathcal{L}_{vee.4}}{\partial\omega} = 0, \quad (2.73)$$

$$\phi: \quad \sum_i g_{i\phi}\rho_{Bi} - m_\phi^2 \left(\frac{\chi}{\chi_0}\right)^2 \phi + \frac{\partial\mathcal{L}_{vee.4}}{\partial\phi} = 0, \quad (2.74)$$

$$\rho: \quad \sum_i g_{i\rho}\tau_3\rho_{Bi} - m_\rho^2 \left(\frac{\chi}{\chi_0}\right)^2 \rho + \frac{\partial\mathcal{L}_{vee.4}}{\partial\rho} = 0, \quad (2.75)$$

where the scalar density is  $\rho_{Si} = \sum_i \bar{\psi}_i \psi_i$  and the baryonic density is  $\rho_{Bi} = \sum_i \bar{\psi}_i \gamma_0 \psi_i$ . The energy momentum tensor is calculated as

$$T_{\mu\nu} = -\mathcal{L}g_{\mu\nu} + \sum_\eta \frac{\partial\mathcal{L}}{\partial(\partial^\mu Q^\eta)} \partial_\nu Q^\eta, \quad (2.76)$$

where  $Q_\eta$  is a generic field and  $g_{\mu\nu}$  is the Minkowski metric tensor

$$g_{\mu\nu} = \text{diag}(1, -1, -1, -1). \quad (2.77)$$

For a perfect fluid, the absence of interactions leaves the energy-momentum tensor diagonal. In the reference frame of the fluid it becomes

$$T_{\mu\nu} = (\epsilon + P)u_\mu u_\nu - P g_{\mu\nu}, \quad (2.78)$$

where the velocity vector field is  $u_\mu = (1, 0)$  and  $u_\mu^2 = 1$ . The energy density and

pressure can be calculated from

$$T_{00} = \epsilon \quad \text{and} \quad T_{ij} = \delta_{ij}p. \quad (2.79)$$



## 3 Neutron Stars

### 3.1 Star Matter

**Symmetric matter** is defined as having the same number of protons and neutrons. Besides that, normally it is also considered infinite, meaning that surface corrections like the ones considered when treating nuclei are not taken into account, without Coulomb repulsion and self-bound. **Star matter** on the other hand is not isospin symmetric, it has many more neutrons than protons. Cooling calculations show that if the amount of protons is higher than  $\sim 10\%$  of the total baryonic number this allows the star to cool faster due to the direct Urca process [42]. This asymmetry is controlled by the isovector mesons  $\rho$  and  $\delta$  that for this reason are extremely relevant for neutron star calculations.

Star matter is also charge neutral

$$\sum_i \rho_{Bi} Q_i = 0, \quad (3.1)$$

where  $\rho_B$  is the number density and  $Q$  is the electric charge for the different baryonic and leptonic species  $i$ . The number density is calculated from

$$\rho_{Bi} = \int d\rho_{Bi} = \int \frac{g}{(2\pi\hbar)^3} f_i d^3k, \quad (3.2)$$

where we used the fact that the correlation between the number density and the distribution function  $f$  is  $\frac{d\rho_{Bi}}{d^3k} = \frac{g}{(2\pi\hbar)^3} f_i$  with  $g$  being the number of states of a particle with momentum  $k$  and  $(2\pi\hbar)^3$  the unit volume of a cell in the phase space. The distribution function is defined as

$$f_i = \frac{1}{e^{(E_i^* - \mu_i^*)/k_B T} + 1}, \quad (3.3)$$

where  $E^*$  and  $\mu^*$  are the energy  $E_i^*(k) = \sqrt{k^2 + m_i^{*2}}$  and the chemical potential

$\mu_i^* = \mu_i - g_{i\omega}\omega - g_{i\phi}\phi - g_{i\rho}\tau_3\rho$  of the different species modified by the medium and  $k_B$  is the Boltzmann constant. At zero temperature all the energy levels are filled up to the Fermi energy so the expression above simplifies to  $f = 1$  for  $E \leq E_F$  and  $f = 0$  for  $E \geq E_F$ . With this, the number density becomes

$$\rho_{B_i} = \int_0^{k_{F_i}} \frac{g}{(2\pi\hbar)^3} d^3k = \frac{gk_F^3}{6\pi^2\hbar^3}. \quad (3.4)$$

The total baryonic density is defined as

$$\rho_B = \sum_i \rho_{B_i}. \quad (3.5)$$

Considering the long time scale for neutron stars, the strangeness quantum number is not constrained and is determined by chemical equilibrium conditions. The chemical equilibrium equations determine the particle composition at each layer of the star. Since there are two conserved quantities, the baryonic number  $\sum_i Q_{B_i} = 0$  and the electric charge  $\sum_i Q_i = 0$ , the chemical potential of all particles can be written as a function of two independent chemical potentials

$$\mu_i = Q_{B_i}\mu_B - Q_i\mu_e, \quad (3.6)$$

where  $\mu_B$  stands for the neutron chemical potential (also known as baryonic chemical potential) and  $\mu_e$  for the electron chemical potential (also known as charged chemical potential). For example, the chemical potential for the protons is

$$\mu_p = \mu_B - \mu_e. \quad (3.7)$$

The reaction associated with it is called  $\beta$ -decay and it reads

$$n \rightarrow p + e + \bar{\nu}_e. \quad (3.8)$$

It determines how and at which rate neutrons can decay into protons and vice-versa. There are two relevant comments to be made at this point. The first one concerns the freedom with which this process can occur. Because the energy levels are occupied up to the Fermi surface, the reaction can only occur if it produces particles with energy

above the threshold. This is called Pauli blocking. It prevents, for example, the neutrons formed during the supernova explosion to decay back into protons. The second point is that there are some correlations between the nucleons that cause some of them to go above the Fermi surface. They are called short range correlations and the holes below the surface created by them can be filled by particles coming from the beta decay. Such change can accelerate the neutron star cooling process [43].

The chemical potentials for the muon and hyperons are

$$\mu_{\mu} = \mu_e, \quad (3.9)$$

$$\mu_{\Lambda} = \mu_B, \quad (3.10)$$

$$\mu_{\Sigma^+} = \mu_B - \mu_e, \quad \mu_{\Sigma^0} = \mu_B, \quad \mu_{\Sigma^-} = \mu_B + \mu_e, \quad (3.11)$$

$$\mu_{\Xi^0} = \mu_B, \quad \mu_{\Xi^-} = \mu_B + \mu_e. \quad (3.12)$$

## 3.2 Inclusion of Gravity

To study the influence of gravity on neutron stars, we analyze how it is balanced by the pressure coming from the equation of state. To do that we first consider the gravitational force acting on a spherical shell with mass  $dM$  at a distance  $r$  from the center of a star with mass  $M$

$$dF_G = \frac{MdM}{r^2}. \quad (3.13)$$

If all mass is assumed to be located at the center of the star that has a density  $\rho$ ,

$$M = \int_0^r dV\rho = \int_0^r 4\pi r'^2 dr'\rho, \quad (3.14)$$

the mass of the infinitesimal part of the shell  $dM$  becomes

$$dM = dV\rho = r^2 \sin\phi dr d\phi d\theta\rho, \quad (3.15)$$

where  $\theta$  is the polar and  $\phi$  the azimuthal angle. Replacing these equations in 3.13, it becomes

$$dF_G = \frac{Mr^2 \sin\phi dr d\phi d\theta\rho}{r^2}. \quad (3.16)$$

On the other hand, the force originating from the pressure  $P$  of the matter inside the shell on the infinitesimal surface area  $dA$  is

$$dF_P = dP dA = dP r^2 \sin \phi d\phi d\theta. \quad (3.17)$$

Stars that do not rotate and are not under the influence of any external force are in hydrostatic equilibrium, meaning that the two forces, gravitational and from the pressure, should balance each other

$$dF_P = -dF_G, \quad (3.18)$$

so that

$$\frac{dP}{dr} = -\frac{M\rho}{r^2}. \quad (3.19)$$

Including relativistic effects in the classical expression for hydrostatic equilibrium, it together with 3.14 become the Tolman-Oppenheimer-Volkov equations (TOV) [9, 10]

$$\frac{dP}{dr} = -\frac{M\rho}{r^2} \left(1 + \frac{P}{\epsilon}\right) \left(1 + \frac{4\pi r^3 P}{M}\right) \left(1 - \frac{2M}{r}\right)^{-1}, \quad (3.20)$$

$$M = \int_0^r 4\pi r'^2 \rho dr'. \quad (3.21)$$

It can be easily seen that these equations have a singularity for  $r = 2M$ . In this way a maximum mass is defined for neutron stars above which they become black holes.

The mass-radius relation of the respective neutron star can be calculated by solving the TOV equations. Because the equations have to be integrated until the radius at which the pressure is zero, or very small compared to the central pressure, the equation of state for the core has to be complemented by one for the crust. We use the one calculated by Baym, Pethick and Sutherland [44] that is constituted by an outer crust of  $^{56}\text{Fe}$  nuclei arranged in a lattice, so as to minimize their Coulomb interaction, with an electron gas and an inner crust of nuclei lattice with electron and neutron gas. Plugging in the EOS for the core, we obtain a different star for each possible central density. The result is shown in Fig. 3-1. But not all the points (stars) are stable configurations.

According to the Le Chatelier principle, that can be written as:

$$\frac{dp}{d\epsilon} \geq 0, \quad \text{or} \quad \frac{dM}{dR} \leq 0, \quad (3.22)$$

the derivative of the star mass with respect to the radius has to be negative. This can be understood as follows: looking at the stable branch we see that if the pressure increases (going left in the Fig. 3-1), the mass would have to increase. Since this cannot happen, the star expands going back to the initial state. If, on the other hand, the pressure decreases (going right in the Fig. 3-1), the mass would have to decrease, but since this cannot happen, the star shrinks back to the original position. On the unstable branch the behavior is different. If the pressure increases (going left), the mass would have to decrease. Since this cannot happen, the star shrinks until it collapses to a black hole. If the pressure decreases (going right), the mass would have to increase, but since this cannot happen, the star expands and dissolves into space.

### 3.3 Different Couplings

Because of its strong influence on neutron star properties, the structure of the self-interaction term of the vector mesons is investigated. In dense systems baryonic vector densities and therewith the mean fields of the vector mesons become especially important for the equation of state of hadronic matter. The fourth-order self-interaction term  $\mathcal{L}_{\text{vec},4}$  of the vector mesons can be written in different forms in a SU(3)-invariant way. To study the difference in the result, three separate coupling schemes are considered,

$$\mathcal{L}_{\text{vec},4} = -g_4[\text{Tr}(V)]^4/4 \quad (\text{a}), \quad -g_4[\text{Tr}(V^2)]^2 \quad (\text{b}), \quad -g_4 2\text{Tr}(V^4) \quad (\text{c}), \quad (3.23)$$

where  $V$  stands for the matrix of the vector meson multiplet shown in the appendix.

The results for the couplings (a) to (c) are shown in Fig. 3-1 for the SU(2) limit of proton, neutron and electron matter. A strong coupling of the  $\omega$  and  $\rho$  meson present in the cases (b) and (c) leads to smaller star masses. In the following calculations the non-linear coupling (a), which does not generate a  $\rho - \omega$  coupling, is used. This allows for more massive neutron stars and is also in general agreement with the observed small mixing of the two mesons. The modification of the original couplings and

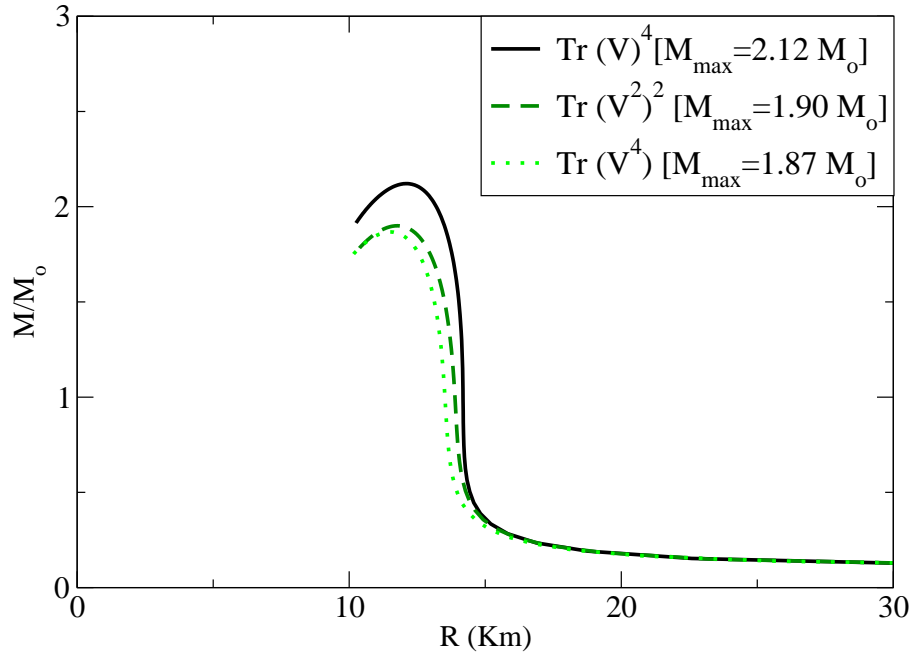


**Figure 3-1:** Star masses versus radii for different vector meson self-interactions. The values of the respective maximum masses are shown.

parameter set of the model used in [12] is done in order to investigate the maximum neutron star masses that can be achieved (similar studies in a different approach have been performed in [45]) while still reproducing hadronic masses in vacuum as well as reproducing phenomenological values of basic nuclear matter ground state properties, as listed in the previous chapter.

### 3.4 Different Compositions

Within the model different situations can be analyzed by including the whole baryon octet or, in addition, the baryon decuplet. As the density increases, the effective baryonic masses decrease and more massive particles can exist. They do not have to appear according to the mass hierarchy because they are also charge, strangeness and isospin dependent. Besides that, the scalar and vector meson interactions entering in the effective masses and effective chemical potentials, respectively, play an important role. Because of these interactions the hyperons appear in chiral models later compared to

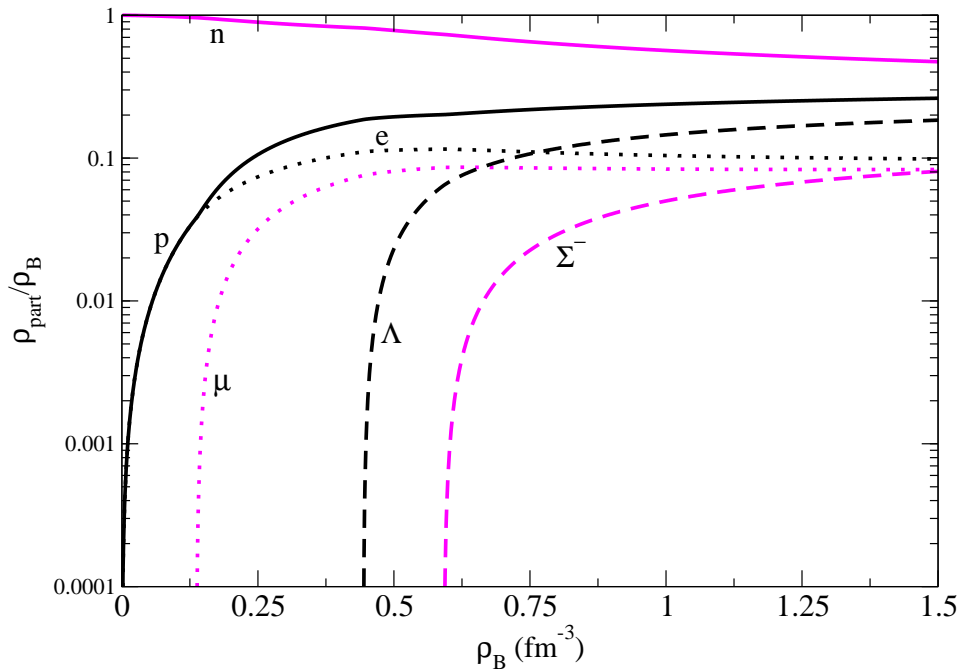


**Figure 3-2:** *The composition of neutron star matter with hyperons.*

Walecka-type models [46, 47]. In practice, the only baryons present in the star besides the nucleons are the  $\Lambda$ ,  $\Sigma^-$  in the first case (Fig. 3-2) and  $\Lambda$ ,  $\Delta^{-,0,+}$  in the second case (Fig. 3-3). In the presence of resonances the  $\Delta^-$  particle replaces the  $\Sigma^-$ , as its effective mass drops faster with density compared to the  $\Sigma^-$ .

As can be seen from Fig. 3-4 the inclusion of new particles, i.e. new degrees of freedom, softens the equation of state (EOS). The same effect would be observed in the symmetric case, when there is no net isospin instead of no net electric charge, in the presence of more massive degrees of freedom. Although the symmetric case has no relevance for neutron stars due to the high intrinsic asymmetry, this case is important for example in heavy ion collisions. The softening of the equation of state causes a decrease of the respective neutron star maximum mass (Fig. 3-5).

Even though all of the different compositions generate massive stars, from now on in this work we will restrict ourselves to the model including the lowest multiplets, i.e. including only the baryon octet, thus avoiding the uncertainties related to the largely unknown coupling strengths of the baryonic decuplet. In this case, it is possible to describe stars with masses higher than  $M = 2M_\odot$  and still take into account

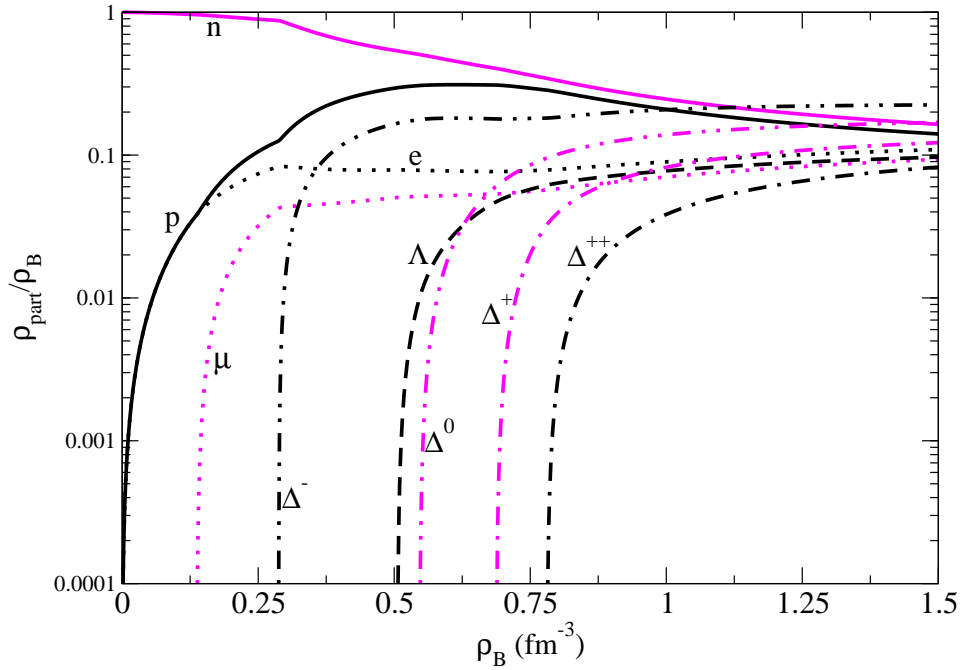


**Figure 3-3:** *The composition of neutron star matter with hyperons and resonances.*

heavy baryonic degrees of freedom. The most massive pulsar observed so far is the PSR J1903+0327 with  $1.74M_{\odot}$  [48]. It was found by the Arecibo telescope in a binary system with a possible main-sequence companion. It has a rotational period of 2.15 ms in a highly eccentric  $e = 0.44$  95-day orbit around the solar mass companion.

### 3.5 Chiral Symmetry Restoration

The transition to the chirally restored phase for any of the considered self-interactions and sets of baryonic degrees of freedom turns out to be a cross over. This effect is intrinsic to this kind of model and is accentuated by the requirement of charge neutrality that makes the different isospin states of baryons with the same vacuum mass appear at different densities in the star, thus smoothing out the effect of their appearance. The chiral restoration can be seen in the behavior of the chiral condensate  $\sigma$  used here as the order parameter for the transition. As it decreases its value, the effective masses of the baryons decrease and they become degenerate. In Fig. 3-6 the normalized condensate is plotted against the star radius showing that in this model the



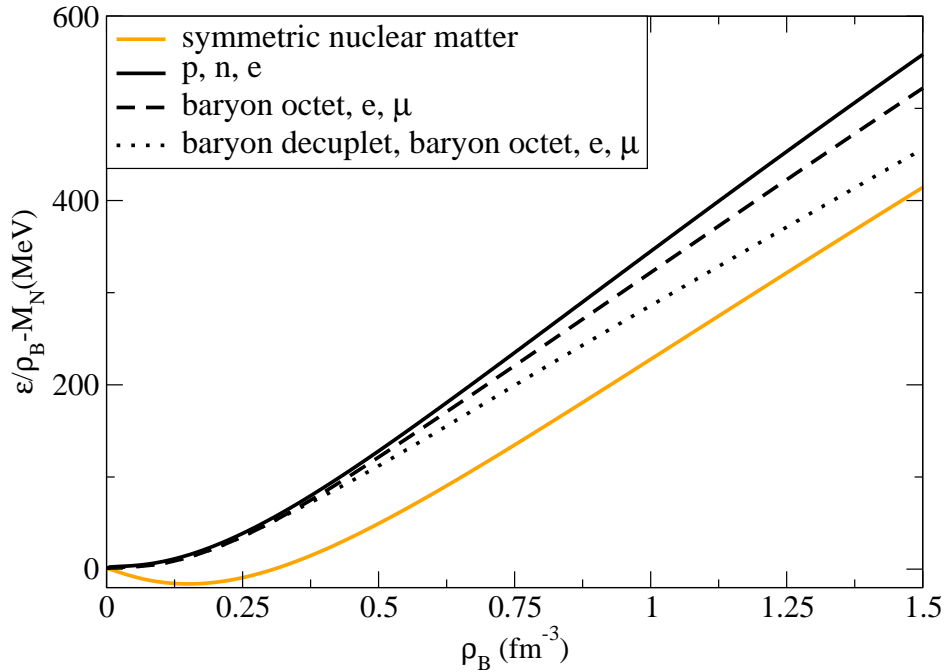


**Figure 3-4:** Binding energy per nucleon versus baryon density for different compositions.

chiral symmetry is partially restored in neutron stars. The reason for the symmetry being only partially restored does not come from the small bare mass term in the effective mass of the baryons (Eq. 2.68) or from the explicit symmetry breaking term included in the Lagrangian density (Eq. 2.67), as one might think, but from the logarithmic terms of the self-interaction for the scalar mesons (Eq. 2.66) [36]. These terms are responsible for reproducing the scale symmetry breaking of QCD but at the same time slow down the chiral symmetry restoration.

A different result was achieved in [49] through the inclusion of heavier resonances as single states with adjustable coupling and degeneracy. Depending on the couplings, a first order phase transition was found to signal the chiral symmetry restoration. This calculation was only done for symmetric matter in order to reproduce the QCD phase diagram. In chapter 6 we reproduce the same structure but also taking into account deconfined states.

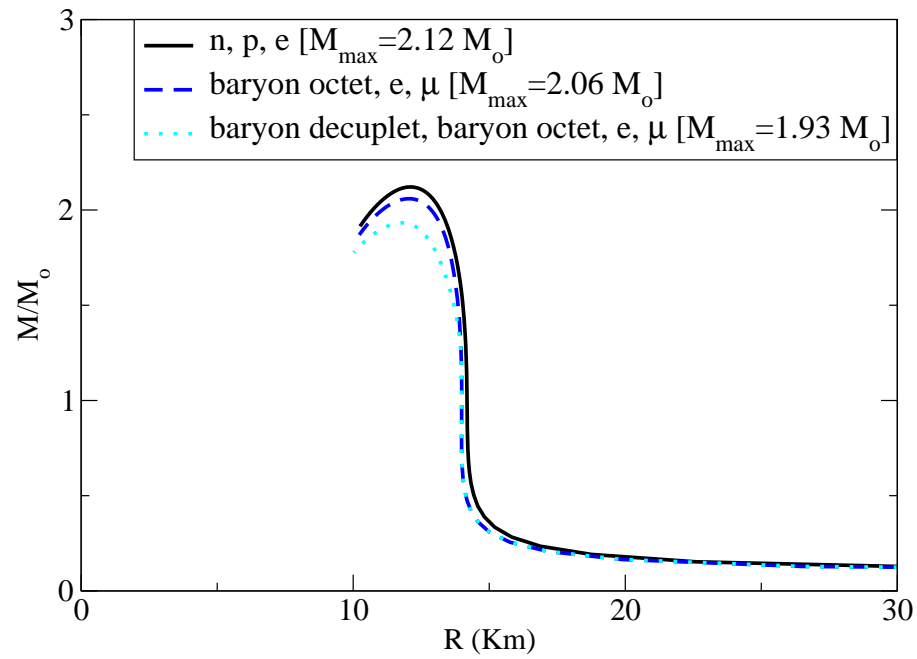


**Figure 3-5:** Star mass versus radius for different compositions. The values of the respective maximum masses are shown.

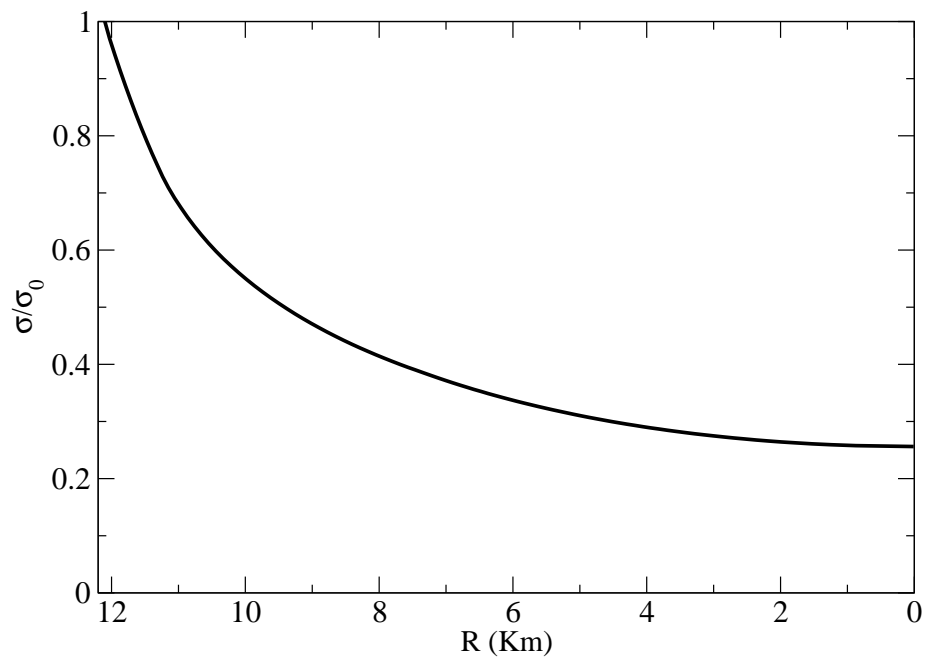


**Figure 3-6:** Normalized scalar condensate versus star radius.

gr

## 4 Proto-Neutron Stars

Right after the supernova explosion, due to the neutronization of the matter, the star contains an abundant number of neutrinos that are trapped in the system. At this point, we cannot take the temperature to be zero, like in later stages of the cooling, because it can reach values of up to 50 MeV in the center of the star. The inclusion of both these features in the model is done in separate steps.

### 4.1 Finite Temperature

In order to determine the matter properties, the thermodynamical potential of the grand canonical ensemble has to be solved. It is defined as

$$\frac{\Omega}{V} = -\mathcal{L}_{\text{scal}} - \mathcal{L}_{\text{vec}} - \mathcal{L}_{\text{SB}} - \mathcal{L}_{\text{vac}} - k_B T \sum_i \frac{g}{(2\pi)^3} \int_0^\infty d^3k \ln(1 + e^{-(E_i^* \mp \mu_i^*)/k_B T}), \quad (4.1)$$

where  $\mathcal{L}_{\text{scal}}$  is the self-interaction term for the scalar mesons,  $\mathcal{L}_{\text{vec}}$  is the self-interaction term for the vector mesons,  $\mathcal{L}_{\text{SB}}$  is the explicit symmetry breaking term,  $\mathcal{L}_{\text{vac}}$  is the vacuum energy (potential at  $\rho_B = 0$  subtracted to give a vanishing energy for the vacuum),  $k_B$  is the Boltzmann constant,  $i$  denotes the fermion type and  $g$  the fermionic degeneracy. At finite temperature, the antiparticles of the fermions are also present in the system and they are taken into account in the thermodynamical potential with a different (positive) sign for the chemical potential. At high temperature the low density regime is mainly controlled by electron-positron pairs.

The baryon density is defined as

$$\rho_B = -\frac{1}{V} \frac{\partial \Omega}{\partial \mu_B} \Big|_{V, T} = \pm \frac{g}{(2\pi)^3} \sum_i \int_0^\infty d^3k \frac{1}{1 + e^{(E_i^* \mp \mu_i^*)/k_B T}}, \quad (4.2)$$

where different signs stand for particles (top) and antiparticles (bottom). The baryonic density, that was a step function in the zero temperature case, becomes here the result

of the sum of these integrals. The entropy per baryon is defined as

$$s = \frac{S}{B} = \frac{S}{V\rho_B} = -\frac{\partial\Omega/\partial T|_{V, \mu}}{V\rho_B}, \quad (4.3)$$

and can also be calculated from the thermodynamic relation

$$s = \frac{\epsilon + P}{T\rho_B} - \frac{\mu_N}{T} - \frac{\mu_{\nu_e} Y_l}{T}, \quad (4.4)$$

where  $\mu_{\nu}$  and  $Y_l$  are the neutrino chemical potential and the lepton number defined in the following. The third term in the equation above is only used for the case of conserved leptonic number.

To study the effect of temperature in neutron stars three different approaches are considered as they have appeared in the literature.

### 4.1.1 Constant temperature

In the simplest case the whole star is considered to have the same temperature. Solving the TOV equations it can be seen that the maximum mass of the neutron star is slightly higher for higher temperatures. This is a balance of two features, the thermal effect on the binding part of the mass (that also contributes to the gravitational mass) and the early onset for the appearance of hyperons. It was already shown in [50] that this effect only continues until a certain temperature.

With increasing density the entropy per baryon remains constant except for small densities as can be seen in Fig. 4-1. This effect comes from the fact that even when the baryon density tends to zero, the electron-positron pairs present at finite temperature still contribute to the pressure and consequently to the entropy.

The transition to the chirally restored phase becomes smoother with the increase of temperature since the jump in the density function becomes smaller. It can be seen in Fig. 4-2 that the chiral symmetry begins to be restored earlier (smaller densities/chemical potentials) for higher temperatures, in agreement with the QCD phase diagram (shown in chapter 6).

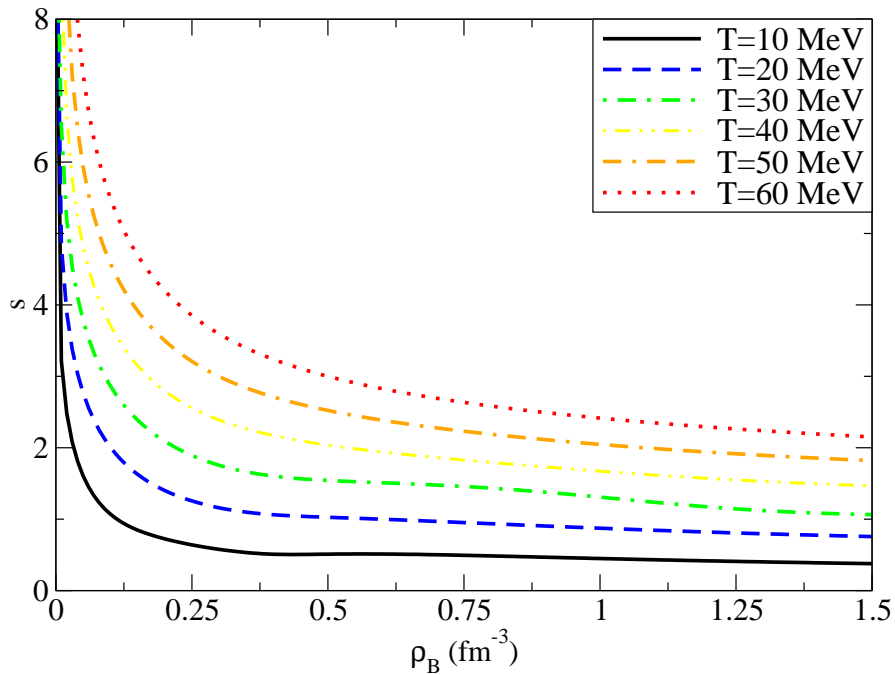


Figure 4-1: Entropy per baryon versus baryon density for different temperatures.

### 4.1.2 Metric dependent temperature

A more complicated but somehow more intuitive case is the one in which the temperature increases toward the center of the star. An interesting approach suggested in [51], defines the temperature at an infinite distance from the star and it increases as the gravitational field created by the presence of the mass of the star becomes higher. In this case  $T = T_\infty / \sqrt{g_{00}}$ , where  $g_{00}$  is the 00 component of the metric tensor that in general relativity is the metric function related to the time coordinate. As the density increases, the temperature also increases (shown in Fig. 4-3 for  $T_\infty = 15$  MeV), but the difference of temperature from the center to the edge of the star is not pronounced. In this case, the maximum mass of the star is also slightly higher for higher temperatures  $T_\infty$ .

### 4.1.3 Constant entropy

In this case the star is considered to have a constant entropy per baryon. Because of this constraint, the temperature is higher in the center of the star (at higher densities)

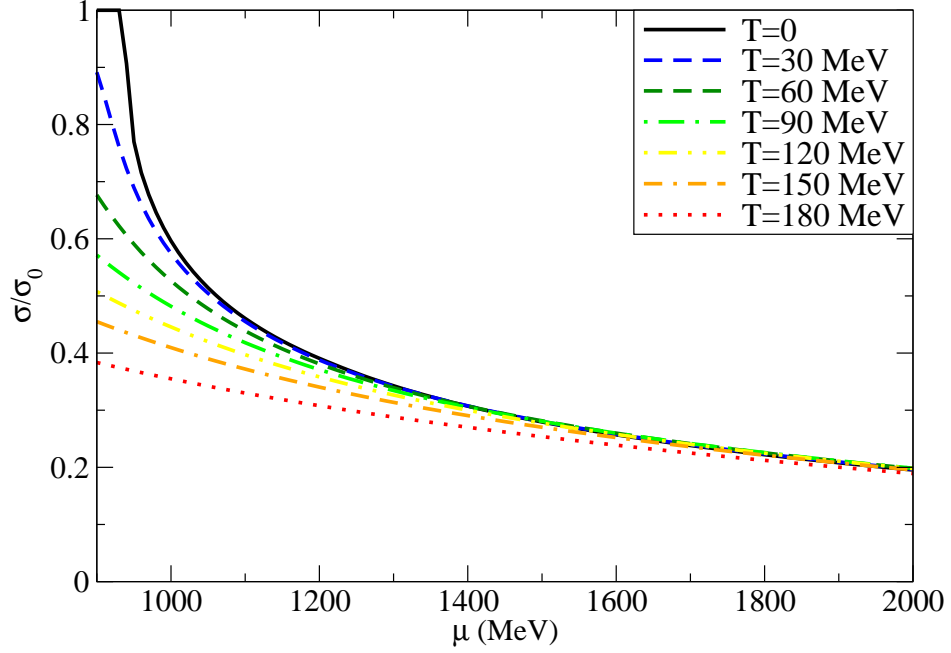


**Figure 4-2:** *Scalar condensate versus chemical potential for different temperatures.*

and lower at the edge, as can be seen in Fig. 4-4. The maximum mass of the star is in this case higher for higher entropies, also because of the thermal effects on the binding part of the mass. This approach agrees with dynamical simulations of the stellar evolution and cooling [52, 53, 54, 55].

## 4.2 Trapped Neutrinos

Another important characteristic of the early moments of the neutron star life is the enormous amount of trapped neutrinos. Their chemical potential  $\mu_\nu$  has to be included in EQ. 3.6 as there is a new conserved quantity in the system, the electron leptonic number  $\sum_i Q_{le_i} = 0$ . It becomes

$$\mu_i = Q_{B_i} \mu_B + Q_i (\mu_{\nu_e} - \mu_e) + Q_{le_i} \mu_{\nu_e}. \quad (4.5)$$

The leptonic number defined as  $Y_l = (\rho_e + \rho_{\nu_e})/\rho_B$  is fixed. In consequence there will be a large number of neutrinos in the star but also an increased electron density. Therefore, demanding charge neutrality, the proton density increases, and with higher

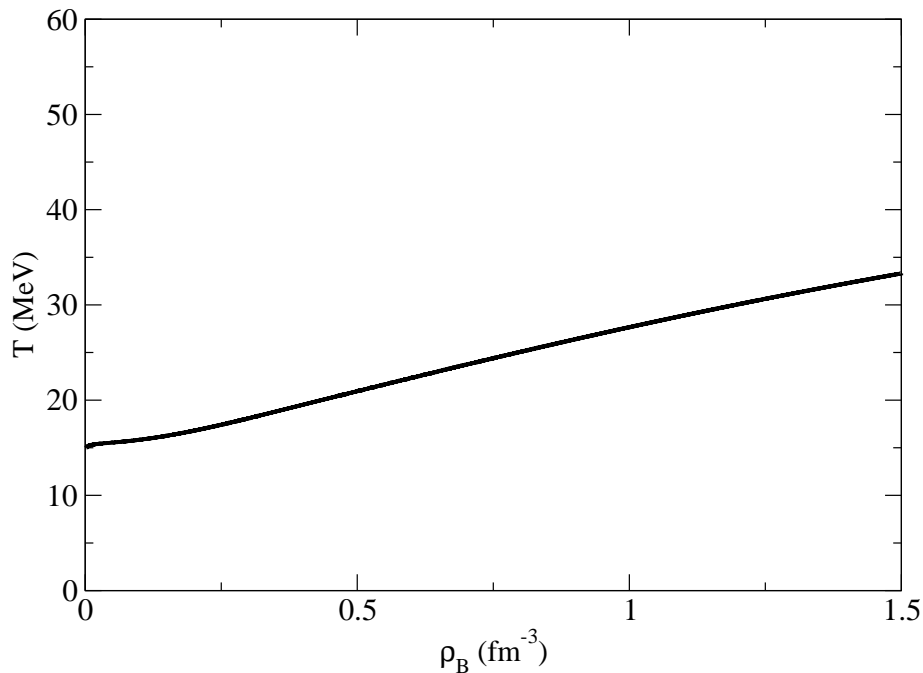


**Figure 4-3:** *Temperature versus baryon density for  $T_\infty = 15$  MeV.*

proton density, the star becomes more isospin symmetric and the neutron Fermi energy decreases. Thus the increase of lepton number softens the EOS and consequently the maximum mass of the neutron star decreases. It is important to keep in mind that this result is dependent on the chosen parameter set and consequently on the particles present in the star. For parameter sets that allow the hyperons to appear at lower densities, the high proton density delays their population allowing the neutron star to be more massive.

### 4.3 Cooling Stages

These two features can be put together to describe the evolution of the star for two extreme cases: constant temperature and quickly increasing temperature throughout the star. After the supernova explosion, the star is still warm so the temperature is fixed to  $T = 30$  MeV or the entropy per baryon is fixed to  $s = 2$ , in which case the temperature increases from 0 at the edge up to 50 MeV in the center (as in Fig.4-4). The star contains a high abundance of neutrinos that were trapped during the

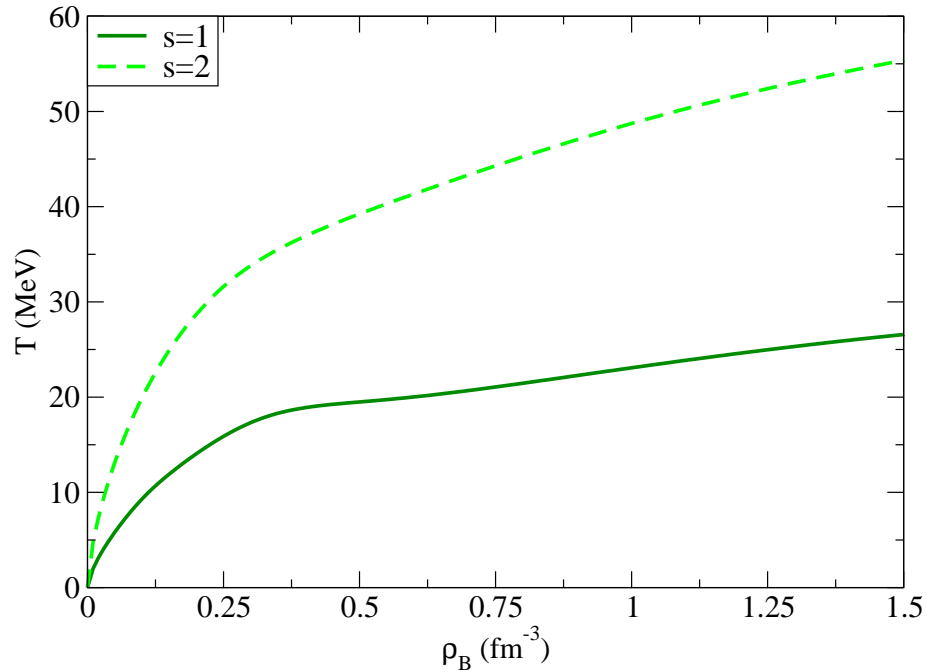


**Figure 4-4:** *Temperature versus baryon density for different entropies per volume per baryon.*

explosion so the lepton number is fixed to a typical value of  $Y_l = 0.4$ . After several seconds (10-20) the neutrinos escape and  $\beta$ -equilibrium is established. After about a minute, the temperature of the star has dropped below 1 MeV via neutrino and photon emission.

The balance between the effects of temperature/entropy and lepton number is very delicate and depends on the parameters of the model. The first line in table 4-1 shows the maximum star masses for different entropies (as suggested in [56]) and different temperatures. As can also be seen in Figs. 4-5 and 4-6 the intermediate step of the evolution with  $s = 2$  and  $\mu_\nu = 0$  is slightly more massive than the first one.

This calculation, though, does not take an important feature into account. The star cannot create or annihilate baryons. They can transform into each other but the total baryon number has to remain fixed. Of course, in the case of stars accreting matter from companions, this restriction is not applicable. If in the earliest stage of the cooling the maximum baryon number that the isolated star could have (according to the TOV equations) was  $B$ , one extra baryon would have made it become unstable



stages	$s = 2$ $Y_l = 0.4$	$s = 2$ $\beta$ equil.	$s = 0$ $\beta$ equil.	$T = 30$ MeV $Y_l = 0.4$	$T = 30$ MeV $\beta$ equil.	$T = 0$ $\beta$ equil.
$M_{\max}(M_{\odot})$	2.05	2.07	2.05	2.08	2.08	2.05
fixed $M_B$	2.05	2.01	1.96	2.08	2.03	1.99
$R(\text{km})$	14.00	15.87	12.44	16.09	17.23	12.33
$M_{\min}(M_{\odot})$	1.07	1.07	0.02	2.02	2.02	0.02
fixed $M_B$	1.07	1.07	0.94	2.02	2.02	1.77

**Table 4-1:** *Maximum masses with and without fixing the baryon number, radii for the maximum masses with fixed baryon number and minimum masses with and without fixing the baryon number for different moments of the star evolution.*

and collapse it into a black hole. For this reason, the later stages of the star have to continue having the same baryon number  $B$  [57]. Following this procedure, and starting with the values of baryon number for the star with  $s = 2$  or  $T = 30$  MeV, respectively, and  $Y_l = 0.4$ , the stable solutions of the colder cases have a smaller mass than the warmer neutrino-rich case. This can be seen in the second line of Table. 4-1. The third line of the table shows the respective radius for the maximum masses of the second line.

According to calculations including finite temperature for quark stars [58, 59], the maximum mass of the star decreases with the increase of temperature. This happens because, in this case, instead of giving extra support against gravity, the thermal energy makes the quarks less bound. It is important to remember that quark stars, differently from neutron stars are self-bound objects. When baryon number is fixed, the results for quark stars are exactly the same as for neutron stars, since in this case there are no extra baryons making the system less bound.

When the shock wave created during the supernova explosion passes through the star, it leaves the outer region with a much higher entropy than the rest. This outer part, that will become the crust, remains warmer for longer time serving as an insulating blanket which delays the star from coming to a complete thermal equilibrium with the interstellar medium. In stars with finite temperature/entropy a crust of high entropy has been used (LLPR compressible liquid drop model for nuclei [60]). In this case the crust is stiff enough to generate massive stars for small central energies resulting in large radii. For the assumption of constant temperature the crust used has an entropy

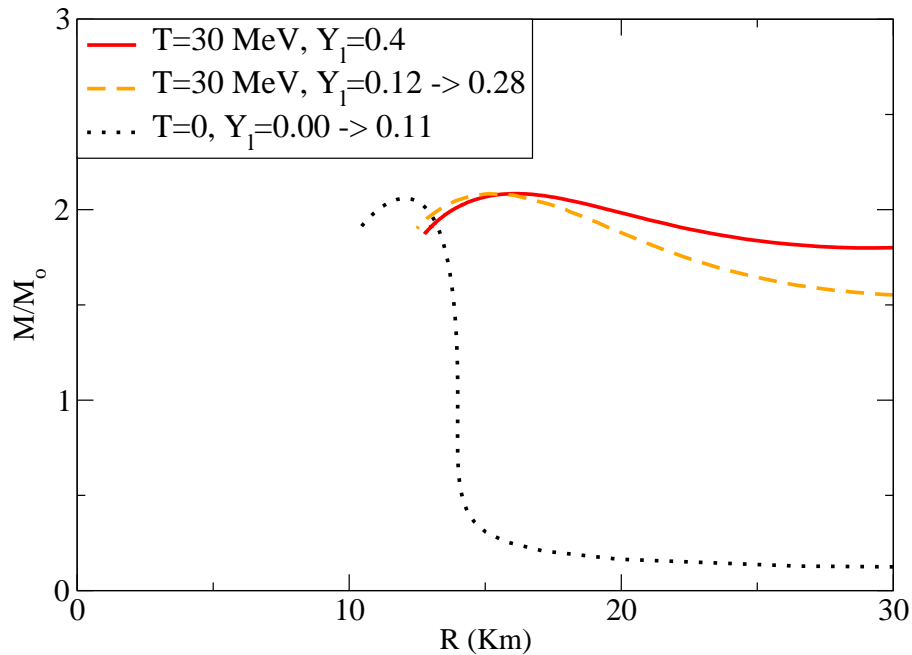


**Figure 4-5:** Star mass versus radius for different stages of the star evolution defined by temperature and lepton number considering the baryon octet,  $e$ ,  $\mu$ .

per baryon  $s = 5$  so that the inner and outer EOS could be continuously connected. For the constant entropy case the crust used has, for the same reason, a value of  $s = 4$ . Similar entropy values are normally used for cooling stages calculations [61, 62].

Because of the use of a warm crust it is also possible to find a minimum mass for each case, shown in the fourth and fifth line of Table 4-1. The pulsar with the smallest observed mass is PSR J1756-2251 with  $M \sim 1.18M_{\odot}$  and a period of 28.5 ms [63]. It is in a binary system with a low mass companion  $M < 1.25M_{\odot}$  having an orbital period of 7.67 hrs and eccentricity of 0.18. The result for the minimum mass found in the constant temperature case is far from the measured value, while the constant entropy one is not. For this reason we conclude that the second option in which the temperature increases toward the interior of the star is the correct one to be used for modeling the cooling stages.

The information obtained from Table. 4-1 also shows how important it is to study different stages of the cooling even if the focus of interest is only the latest stage. As it was shown, the maximum mass that an isolated cold star can have is directly dependent on the mass of the warm star with trapped neutrinos and these masses are

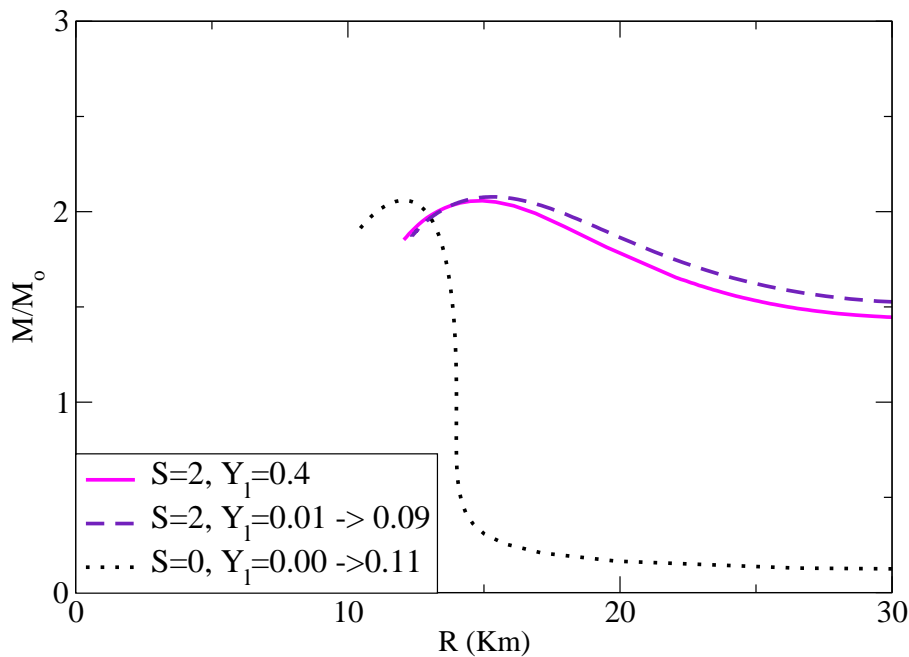


**Figure 4-6:** Star mass versus radius for different stages of the star evolution defined by entropy and lepton number considering the baryon octet,  $e$ ,  $\mu$ .

related through fixed baryonic number. The stars with mass between the values of lines 1 and 2 of Table. 4-1 can only exist if they accrete mass from a companion star, and thus increase their baryon number.

## 4.4 Meson Condensation

According to the Fermi principle, at any temperature, only two fermions (spin 1/2) can occupy each state. Bosons at low temperatures, on the other hand, can reach a state in which all particles collapse into the lowest quantum state. It is called Bose-Einstein condensation and was first predicted by Satyendra Nath Bose and Albert Einstein in 1924-25 [64, 65]. Seventy years later, the first gaseous condensate was produced by Eric Cornell and Carl Wieman in 1995 at the University of Colorado, using a gas of rubidium atoms cooled to 170 nanokelvin and they won the 2001 Nobel Prize for the achievement. This phenomenon can also happen in neutron star cores. At a certain density the mesons condense and stop contributing to the pressure of the system

causing a substantial softening of the equation of state. This effect, in general, causes the neutron stars to become unstable or to have low mass.

The process of kaon condensation was already studied within the chiral model [66, 67]. It was also applied to proto-neutron stars using other models in [68, 69]. We intend here to analyze the onset of kaon condensation in our model with the present coupling and parametrization at different stages of the cooling. This can be done by analyzing when the chemical potential of the kaons becomes higher than their in-medium energies at zero momentum. The baryons couple directly with kaons and antikaons, which causes their effective masses to reduce with density. This happens because of the strongly attractive  $K^-$ -baryon interaction in dense matter. Consequently, the in-medium energy  $\omega$  also decreases with density

$$\omega_k = \left\{ -\frac{1}{4f_k^2} [3(\rho_p + \rho_n) + (\rho_p - \rho_n)] + \left\{ \frac{1}{16f_k^4} [3(\rho_p + \rho_n) + (\rho_p - \rho_n)]^2 \right. \right. \\ \left. \left. -4 \left[ 1 - \frac{1}{f_k} (\sigma' + \sqrt{2}\zeta' + \delta') + \frac{d_1}{2f_k^2} (\rho_{Sp} + \rho_{Sn}) + \frac{d_2}{2f_k^2} [(\rho_{Sp} + \rho_{Sn}) + (\rho_{Sp} - \rho_{Sn})] \right] \right. \right. \\ \left. \left. \left[ -m_k^2 + \frac{m_k^2}{2f_k} (\sigma' + \sqrt{2}\zeta' + \delta') \right] \right\}^{\frac{1}{2}} \right\} / \\ \left\{ 2 - \frac{2}{f_k} (\sigma' + \sqrt{2}\zeta' + \delta') + \frac{d_1}{f_k^2} (\rho_{Sp} + \rho_{Sn}) + \frac{d_2}{2f_k^2} [(\rho_{Sp} + \rho_{Sn}) + (\rho_{Sp} - \rho_{Sn})] \right\}, \quad (4.6)$$

with  $\sigma'$ ,  $\zeta'$  and  $\delta'$  being  $(\sigma - \sigma_0)$ ,  $(\zeta - \zeta_0)$  and  $(\delta - \delta_0)$ , respectively and  $d_1$  and  $d_2$  coupling constants. Here, for simplicity, only the nucleons were considered because of the hyperons later appearance. See [66] for details.

The net effect of  $K^-$  condensation in neutron star matter is that  $K^-$  condensate replaces electrons in maintaining charge neutrality. The onset of  $\bar{K}^0$  condensation is higher than for the  $K^-$  and because of the repulsive optical potential for  $K^+$  and  $K^0$ , their condensation is unlikely to happen in (proto-)neutron stars. For cold hyperonic matter, the onset of  $K^-$  condensation happens at  $\rho_B = 0,74\text{fm}^{-3}$ , while the central density in the most massive neutron star allowed is  $\rho_c = 0,91\text{fm}^{-3}$ . If there is no further contribution for the star mass after kaon condensation occurs, the maximum mass is reduced from  $M_{\text{max}} = 2.06M_\odot$  to  $M_{\text{max}} = 2.04M_\odot$ . Actually, this reduction

is even smaller because although after condensation there are no further changes in the pressure, there are indirect changes on the fields that give contributions to the stellar mass.

Increasing the temperature/entropy and lepton number only delays the appearance of the condensation. Putting these features together, the condensation onset will happen at densities much higher than the ones present in neutron stars. Based on this we conclude that kaon condensation does not affect our approach to study neutron star cooling through the analysis of different stages.



## 5 Rotational Effects

Neutron stars rotate with a period that ranges between 8.5 seconds and the incredible value of 1.4 milliseconds. At such angular velocities, it is expected that rotation modifies neutron star properties. In this chapter we will analyze what these modifications are and which new constraints they bring to the cooling process.

### 5.1 Formalism

The rotation of a star, like every non-rigid body, causes deformations. The measurement of the deformation is called eccentricity and it is defined as  $e = \sqrt{1 - R_{\text{pole}}^2/R_{\text{equator}}^2}$ . It is zero for a sphere and  $e = 1$  for a disc. When rotating the neutron star, considered spherical so far, becomes flat on the poles, and the faster it rotates the higher is its eccentricity. To be able to include such an effect in the hydrostatic equilibrium equations, there should be a polar coordinate  $\theta$  dependence on the metric of the star. In the TOV equations only the radial coordinate  $r$  is taken into account, indicating that they cannot be used for rotating bodies.

The rotation provides extra stability for the star against gravitational collapse. The faster the star rotates, the more massive it can be [70]. Since the rotational frequency modifies the space-time, it is clear that the metric of the star has also to depend on it. Effects concerning the dragging of the local inertial frames also have to be taken into account. This effect generates centrifugal forces that do not originate from interactions with other bodies, but from the rotation of the frame of reference within which the stellar matter resides.

We will adopt in this work the formalism derived in [11] that is based on the Hartle's approximation [71] including corrections up to second order. The results using this approach will later on be compared with full calculations. The metric in spherical coordinates of a rotating, axially symmetric (with respect to the azimuth angle  $\phi$ ) star is

$$ds^2 = e^{2\tau}(dt)^2 - e^{2\Phi}(d\phi - \Omega dt)^2 - e^{2\Theta}(d\theta)^2 - e^{2\rho}(dr)^2, \quad (5.1)$$

where  $\tau$ ,  $\Phi$ ,  $\Theta$  and  $\rho$  depend on the radial coordinate  $r$ , polar angle  $\theta$  and the star angular velocity  $\omega$ . The quantity  $\Omega$  denotes the angular velocity of the local inertial frame and also depends on  $r$ ,  $\theta$  and  $\omega$ .

To simplify the treatment of rotating stars, we make use of perturbation theory. In this case the changes due to rotation in the perfect fluid energy momentum tensor are

$$T_{\mu\nu} \equiv T_{\mu\nu}^0 + \Delta T_{\mu\nu}, \quad (5.2)$$

where

$$T_{\mu\nu}^0 \equiv (\epsilon + P)u_\mu u_\nu - P g_{\mu\nu}, \quad (5.3)$$

$$\Delta T_{\mu\nu} \equiv (\Delta\epsilon + \Delta P)u_\mu u_\nu - \Delta P g_{\mu\nu}. \quad (5.4)$$

The quantities  $P$  and  $\epsilon$  are pressure and energy density measured by an observer in the local inertial frame comoving with the fluid. The quantities  $\Delta P$  and  $\Delta\epsilon$  are the lowest order from a multipole expansion

$$\Delta P = (\epsilon + P)(p_0 + p_2 P_2 \cos \theta), \quad (5.5)$$

$$\Delta\epsilon = \Delta P \frac{\partial \epsilon}{\partial P}, \quad (5.6)$$

where  $p_0$  is a monopole contribution ( $l = 0$ ),  $p_2$  is a quadrupole contribution ( $l = 2$ ) and  $P_2 \cos \theta$  is a second order Legendre polynomial. The metric functions  $\tau$ ,  $\Phi$  and  $\Theta$  ( $r$ ,  $\theta$  and  $\omega$ ) are expanded up to second order in the star's rotational frequency  $\omega$ .

The star's moment of inertia becomes in this approach

$$I = 2\pi \int_0^\pi d\theta \int_0^R dr e^{\tau+\Phi+\Theta+\rho} \frac{\epsilon + P}{e^{2\tau-2\Phi} - \bar{\omega}^2} \frac{\bar{\omega}}{\omega}, \quad (5.7)$$

where  $\bar{\omega} = \omega - \Omega$  is the angular velocity of the fluid relative to the angular velocity of the local inertial frame. The relativistic expression for the baryon number of a star is

$$B = 4\pi \int_0^R dr r^2 \frac{\rho}{\sqrt{1 - 2M(r)/r}}, \quad (5.8)$$



and the change in it due to rotation is

$$\Delta B = \frac{m_0}{m_N} + \frac{4}{m_N} \pi \int_0^R dr r^2 \left\{ (\epsilon + P) p_0 \left[ \frac{\partial \epsilon}{\partial P} \left( \frac{1}{\sqrt{1-2M(r)/r}} - 1 \right) - \frac{\partial \epsilon_{\text{int}}}{\partial P} \frac{1}{\sqrt{1-2M(r)/r}} \right] + \frac{(\epsilon - \epsilon_{\text{int}})}{\sqrt{1-2M(r)/r}} \left( \frac{m_N}{r} + \frac{1}{3} (jr\bar{\omega})^2 \right) - \frac{1}{4\pi r^2} \left[ \frac{1}{12} (jr^2 \frac{d\bar{\omega}}{dr})^2 - \frac{1}{3} \frac{dj}{dr} r^3 \bar{\omega}^2 \right] \right\}, \quad (5.9)$$

where  $m_0$  is the monopole contribution to the mass,  $M(r)$  is the mass at the radius  $r$ ,  $\epsilon_{\text{int}} = \epsilon - m_N \rho_B$  is the internal energy and  $j$  is defined as  $j = \frac{\sqrt{1-2M(r)/r}}{\sqrt{1-2M/r}}$  with  $M$  being the total mass of the star.

## 5.2 Kepler Frequency

For every non-rigid rotating body there is an angular velocity limit beyond which matter starts to be expelled on the equatorial line. In neutron stars this limit was named after the physicist Johannes Kepler. Classically, it is calculated equating the gravitational force holding a body on a spherical surface to the centrifugal force pushing it out in the direction normal to the surface:  $\omega_K = \sqrt{\frac{M}{R^3}}$ . The relativistic expression for this quantity including monopole and quadrupole corrections is

$$\omega_K^2 = \left[ 1 + (1 + \eta_1) \left( \frac{\Omega}{\omega} \right) - (2 + \eta_2) \left( \frac{\Omega}{\omega} \right)^2 \right]^{-1} \frac{M}{R^3}, \quad (5.10)$$

with  $\eta_1$  and  $\eta_2$  defined as

$$\eta_1 = \frac{5}{2} \left( 1 + \frac{2}{5} \frac{R}{M_s} \right) R^2 \Omega^2, \quad (5.11)$$

$$\eta_2 = \eta_1 + \frac{1}{2} \left( 1 + \frac{1}{4} \frac{R}{M_s} \right) R^2 \Omega^2 \left( \frac{\omega^2}{\Omega^2} - 1 \right) - \frac{3}{2} \left( 1 + \frac{5}{6} \frac{M_s}{R} - \frac{1}{4} \frac{R}{M_s} \right), \quad (5.12)$$

and  $M_s$  is the respective static star mass.

The relativistic value of the Kepler limit for the angular velocity is approximately 70% of the value in the classical limit.

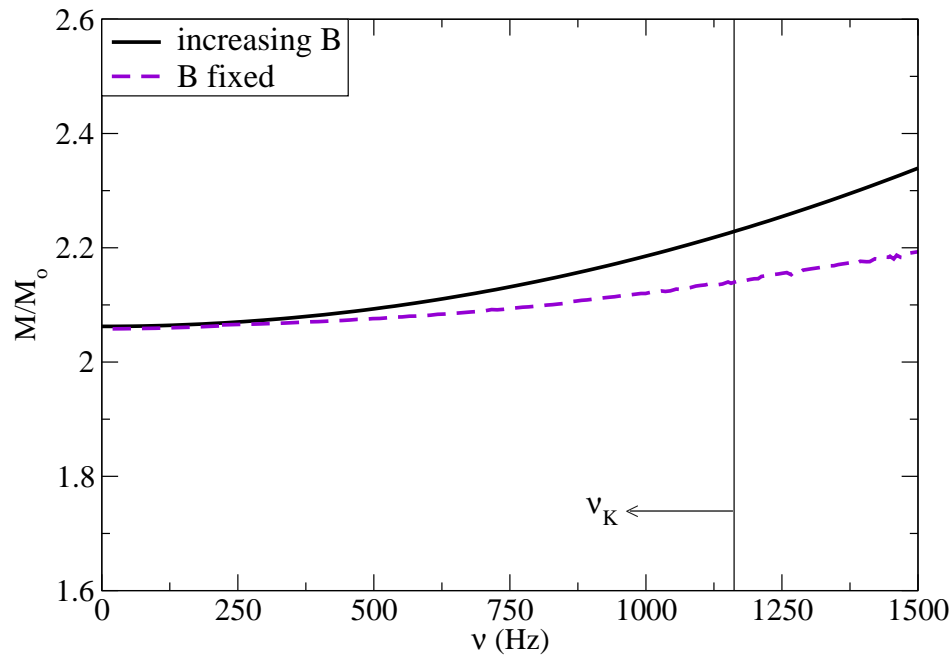


**Figure 5-1:** Star mass versus rotational frequency with and without fixing the baryonic number.

### 5.3 Modification on Stars

The maximum mass that a neutron star can hold against gravity is modified by rotation. The faster the star rotates, the higher is its mass and radius. This increase of the mass is in part caused by a larger possible baryonic number. If we fix  $B$  when increasing the rotational frequency of the star from  $\nu = 0$  to  $\nu = \nu_K = \omega_K/2\pi$ , the increase in the mass due to rotation decreases from 15% to 5% (Fig. 5-1). The first case can be identified as a star accreting mass from a companion and speeding up. The second case can be identified with the spin down of an isolated cold star with a certain baryon number (in this case  $2.8 \times 10^{57}$  baryons) that continues until it emits all its energy and stops rotating.

The Kepler frequency calculated in this case is  $\nu_K = 1162,03$ . This value is above the frequency suggested for the pulsar XTE J1739-285, believed to have a frequency of  $\nu = 1122$  Hz when observed in 2007 [72]. However, this result is not currently statistically significant. The next candidate for fastest pulsar is the PSR J1748-2446ad with  $\nu = 716$  Hz observed in 1982 [3].

stages		$s = 2$ $Y_l = 0.4$ $\nu = \nu_K$	$s = 2$ $\beta$ equil. $\nu = \nu_K$	$s = 0$ $\beta$ equil. $\nu = \nu_K$	$s = 0$ $\beta$ equil. $\nu = 0$
free B	$\nu_K$ (Hz)	1452.56	1424.48	1515.86	0
	$M_{\max}$ ( $M_\odot$ )	2.31	2.33	2.34	2.06
fixed B	$\nu_K$ (Hz)	1228.23	1110.28	1162.03	0
	$M_{\max}$ ( $M_\odot$ )	2.25	2.19	2.14	2.06
fixed B/L	$\nu_K$ (Hz)	1195.30	1095.90	1162.03	
	$M_{\max}$ ( $M_\odot$ )	2.24	2.19	2.14	

**Table 5-1:** Maximum frequencies and masses with and without fixing  $M_B$  and  $L$  for different stages of the cooling.

In order to analyze the applicability of the approximation used in this work, we compare our results with a full calculation [73]. The difference in the mass predicted for the neutron star at the frequency of 716 Hz is less than 1%. This shows that the formalism used here is reasonable for the range of frequencies observed in neutron stars.

## 5.4 Constraints for the Cooling

We consider the rotational effects on cooling from the very first stage of the neutron star life to the last one, when the star stops rotating. In this case, the baryon number is fixed by the last stage, instead of the first one like in the previous chapter, because the rotation always increases the allowed baryon number. Table. 5-1 shows the Kepler frequency and the respective maximum mass for each stage of the cooling in the first two lines. In the third and fourth lines the same quantities are shown but now constrained to the baryonic number of the cold non-rotating case. If we further consider that the angular momentum is conserved through the first seconds of the neutron star evolution, the resulting allowed maximum frequencies and masses are showed in the fifth and sixth lines. In the last case, the angular momentum is constrained by the cold case.

The angular momentum is calculated through  $J = I\omega$  taking into account the deformation caused by rotation and the dragging of local inertial frames. Considering

that the star is axially-symmetric and the neutrino emission on the neutron star is axially-symmetric, angular momentum is conserved. This assumption is normally made for the first seconds of the neutron star evolution [62, 74]. As the star cools down, its maximum allowed radii and masses change (Tab. 4-1). This is compensated by the rotational frequency of the star [57]. If the star is not axially-symmetric there will be angular momentum loss during the cooling phase due to the emission of gravitational waves. If the neutrino emission is not axially-symmetric there will be angular momentum loss during the deleptonization process.

The Table. 5-1 shows that independent of including angular momentum conservation or not, during the first seconds of the evolution, there are some frequencies allowed before, but not after deleptonization. In this case the star has to spin down in order to remain stable. The stars with mass and frequency between the values of lines 1,2 and 3,4 can exist at the first stage but cannot continue cooling to the last stages. They necessarily collapse to black holes during the process unless they accrete mass from a companion. In this case the baryonic number would increase and higher maximum masses would be possible. Gravitational collapse to black holes could be observed by the sudden suppression of neutrinos coming from the star.

## 6 Hybrid Stars

Although the chiral model predicts a phase with partially restored chiral symmetry, the only degrees of freedom present in the system so far are hadrons. In this chapter we perform modifications to the chiral model in order to include quark degrees of freedom. We introduce a mechanism that controls which particles are present at which density through, among other things, the potential for the deconfinement order parameter. This potential, originally developed to be used for lattice QCD at zero or low chemical potential and high temperature, is modified to also be used in the limit of high chemical potential and low temperature, relevant for neutron stars.

We use constraints from both limits and also knowledge of the phase diagram to calibrate the model. With the model ready we can make calculations for any density and temperature as for example heavy ion collisions or proto-neutron stars.

### 6.1 Motivation

The idea of quark stars was suggested for the first time by Itho in 1970 [75]. Since then there were many advances in the field, especially with the development of QCD. The models used to describe neutron stars nowadays can generally be divided into two classes. The first class includes approaches in which the constituent particles are hadrons [76, 77, 46]. Some of them incorporate certain symmetries from QCD, like chiral symmetry, but they do not include deconfinement. Examples of these are hadronic sigma models [12, 38, 78, 36]. The second class includes quark star models, which usually do not directly incorporate hadronic degrees of freedom in the formulation. Examples of these are bag-model studies [79] as well as quark-NJL model and quark sigma-models [80].

Using these approaches hybrid neutron stars, which consist of hadronic and quark phases, are normally described by adopting two different models with separate equations of state for hadronic and quark matter (see e.g. [81]). They are connected at the chemical potential in which the pressure of the quark EOS exceeds the hadronic one,

signalling the phase transition to quark matter.

## 6.2 The Modified Model

Within our approach we employ a single model for the hadronic and quark phases. The extension of the model to quark degrees of freedom is constructed in a spirit similar to the Polyakov NJL model [82], in the sense that it is a non-linear sigma model that uses the Polyakov loop  $\Phi$  as the order parameter for deconfinement. This is a quite natural idea, since the Polyakov loop is related to the  $Z(3)$  symmetry, that is spontaneously broken by the presence of quarks. It is defined as a thermal Wilson line winding around the imaginary time direction with periodic boundary conditions and it reads

$$\Phi = \frac{1}{3} \text{Tr}[\mathcal{P} e^{i \int_0^{1/T} d\tau A_4}] = \frac{1}{3} \text{Tr} e^{i\Phi/T}, \quad (6.1)$$

where  $\mathcal{P}$  denotes path ordering,  $A_4 = iA_0$  is the temporal component of the  $SU(3)$  gauge field and  $\phi$  is the background color gauge field in which the quarks move. In a convenient gauge (called Polyakov gauge) the matrix  $\phi$  has a diagonal representation

$$\phi = \phi_3 \lambda_3 + \phi_8 \lambda_8, \quad (6.2)$$

which leaves only two independent variables,  $\phi_3$  and  $\phi_8$  that are necessarily real quantities in order to sustain the unitarity of the group.

The conjugate of the Polyakov loop is

$$\Phi^* = \frac{1}{3} \text{Tr}[\mathcal{P} e^{-i \int_0^{1/T} d\tau A_4}] = \frac{1}{3} \text{Tr} e^{-i\Phi/T}. \quad (6.3)$$

At zero chemical potential  $\Phi^* = \Phi$  due to the charge conjugation invariance. At finite chemical potential  $\Phi^*$  is always higher than  $\Phi$  and the difference is higher around phase transitions [83]. For simplicity we consider  $\Phi^* = \Phi$  for a first investigation of the model.

The lagrangian density of the non-linear sigma model in mean field approximation Eq. 2.63 becomes:

$$\mathcal{L}_{\text{MFT}} = \mathcal{L}_{\text{Kin}} + \mathcal{L}_{\text{int}} + \mathcal{L}_{\text{scal}} + \mathcal{L}_{\text{vec}} + \mathcal{L}_{\text{SB}} - \mathcal{U}, \quad (6.4)$$

where the terms represent the kinetic energy term for hadrons, quarks, and leptons, the interactions between baryons (and quarks) and vector and scalar mesons, the self-interactions of scalar and vector mesons and an explicitly chiral symmetry breaking term. The Polyakov-loop potential  $\mathcal{U}$  will be discussed in the following. Finite-temperature calculations include the heat bath of hadronic and quark quasiparticles within the grand canonical potential of the system.

The effective mass for the baryons is the same as in Eq. 2.68 except for an additional term containing the Polyakov field  $\Phi$ :

$$m_b^* = g_{b\sigma}\sigma + g_{b\delta}\tau_3\delta + g_{b\zeta}\zeta + \delta m_b + g_{b\Phi}\Phi^2. \quad (6.5)$$

The effective mass for the quarks is analogously defined with  $\delta m_{u,d} = 5$  MeV and  $\delta m_s = 150$  MeV.

$$m_q^* = g_{q\sigma}\sigma + g_{q\delta}\tau_3\delta + g_{q\zeta}\zeta + \delta m_q + g_{q\Phi}(1 - \Phi). \quad (6.6)$$

The Polyakov loop assumes non-zero values with the increase of temperature/density. Due to its presence in the baryons effective mass and the high related coupling constant, it suppresses the baryons at the referred limit. On the other hand, the Polyakov loop presence in the effective mass of the quarks, included with a negative sign, insures that no quarks will be present at low temperatures/densities.

The developed potential for the Polyakov loop  $\mathcal{U}$  is

$$\mathcal{U} = (\alpha_0 T^4 + \alpha_1 \mu^4 + \alpha_2 T^2 \mu^2) \Phi^2 + \alpha_3 T_0^4 \ln(1 - 6\Phi^2 + 8\Phi^3 - 3\Phi^4). \quad (6.7)$$

It is based on [84, 85] and adapted to include terms that depend on the chemical potential, in order to reproduce the main features of the phase diagram at high densities.

The new coupling constants for the quarks are  $g_{q\omega} = 0$ ,  $g_{q\phi} = 0$ ,  $g_{q\rho} = 0$ ,  $g_{q\sigma} = -3.0$ ,  $g_{q\delta} = 0$ ,  $g_{q\zeta} = -3.0$ ,  $T_0 = 200$  MeV,  $\alpha_0 = 1.85$ ,  $\alpha_1 = 1.44 \times 10^{-3}$ ,  $\alpha_2 = 0.08$ ,  $\alpha_3 = 0.40$ ,  $g_{N\Phi} = 1500$  MeV and  $g_{q\Phi} = 500$  MeV. They are chosen to reproduce QCD lattice data, including a first order phase transition for pure gauge at  $\mu = 0$  at  $T = T_0 = 270$  MeV, and known information about the phase diagram. This includes a crossover for both chiral symmetry restoration and deconfinement to quark matter at small chemical potential. For vanishing chemical potential the transition

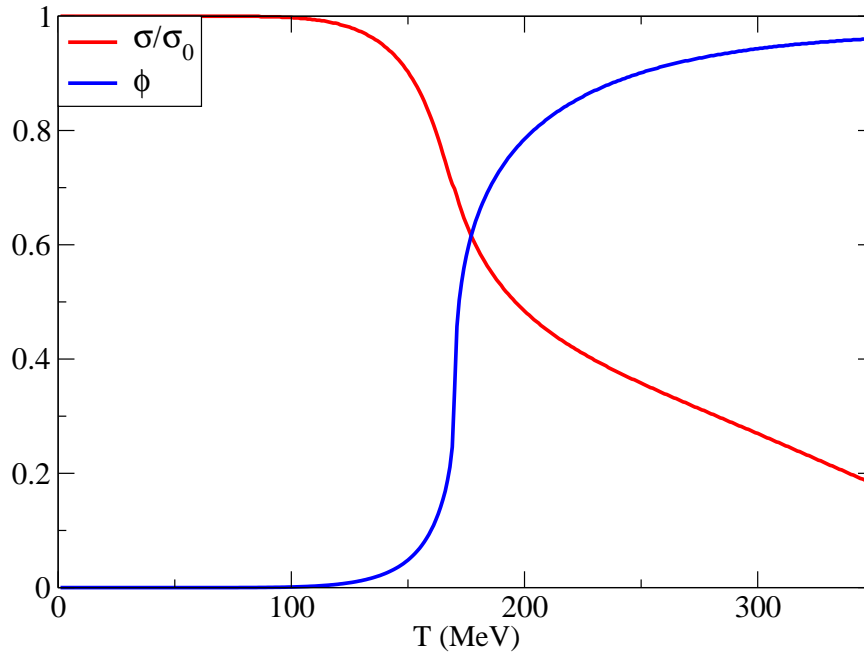


**Figure 6-1:** Order parameters for chiral symmetry restoration and deconfinement to quark matter for symmetric matter at zero chemical potential.

temperature is 171 MeV, determined as the peak of the change of the chiral condensate and the Polyakov loop (Fig. 6-1).

### 6.3 The Phase Diagram

The QCD phase diagram constructed using the model is shown in Fig. 6-2 for symmetric as well as for star matter. The transition from hadronic to quark matter is a crossover for small chemical potentials. Beyond the critical end-points, situated at  $\mu_c = 354$  MeV and  $T_c = 167$  MeV for symmetric matter (in accordance with [86]) and at  $\mu_c = 371$  MeV and  $T_c = 166$  MeV for star matter, a first order transition line for deconfinement begins. The critical temperatures for chiral symmetry restoration coincide with the ones from deconfinement. Each phase contains hadrons and quarks in higher or lower quantity except for the zero temperature case, in which there is no mixing. For star matter the first order transition line ends up at the zero temperature axis at  $\mu_B = 1345$  MeV, that is equivalent to four times saturation density.



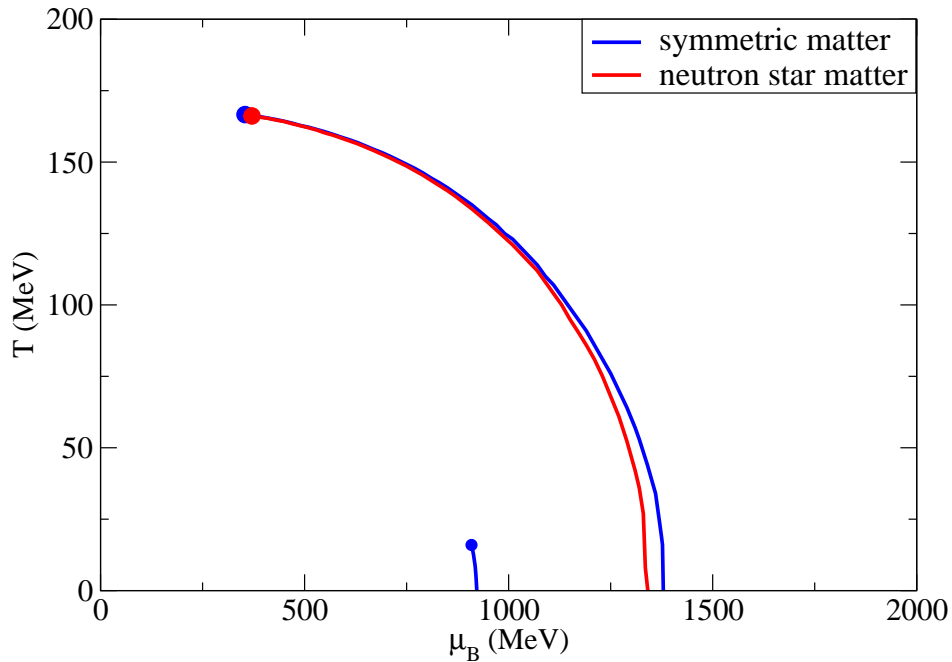


**Figure 6-2:** Phase diagram. The lines represent first order transitions for symmetric and star matter. The circles mark the respective critical end-points.

Since the model is able to reproduce nuclear matter saturation at realistic values for the saturation density, nuclear binding energy, as well as as compressibility and asymmetry energy, we calculate the nuclear matter liquid-gas phase transition. It has a critical point at  $\mu_c = 909$  MeV and  $T_c = 16$  MeV.

In order to reproduce heavy ion collision conditions, two new features are included. The first one are mesons, pions and kaons, that are largely produced at high temperatures and small chemical potentials due to their small masses. For simplicity they are taken in this first approach as having constant mass. The second feature is the inclusion of a strange chemical potential in order to conserve strangeness  $\sum_i Q_{S_i} = 0$ . It modifies Eq. 4.5 to

$$\mu_i = Q_{B_i} \mu_B + Q_i (\mu_{\nu_e} - \mu_e) + Q_{l_{e_i}} \mu_{\nu_e} + Q_{S_i} \mu_S. \quad (6.8)$$

The chemical potentials for the quarks are

$$\mu_u = \frac{1}{3} \mu_B - \frac{2}{3} \mu_e, \quad (6.9)$$

$$\mu_d = \frac{1}{3}\mu_B + \frac{1}{3}\mu_e, \quad (6.10)$$

$$\mu_s = \frac{1}{3}\mu_B + \frac{1}{3}\mu_e - \mu_S, \quad (6.11)$$

where  $\mu_e$  is nonzero only for star matter.

## 6.4 Hybrid Stars

For hybrid star calculations the new features included to obtain the phase diagram are not relevant. At very high chemical potential the production of baryons dominates over the mesons and on the long time scale of neutron stars strangeness is not conserved. At this point, only the last stages of the cooling are considered, when the star is already cold and deleptonized, so the neutrino chemical potential is zero and the leptonic number is not conserved. There are two different options for how to proceed with the quantities that are conserved at the phase transition.

### 6.4.1 Local charge neutrality

The first option is to consider that both hadronic and quark phases are separately in beta equilibrium and charge neutrality. This procedure is called Maxwell construction and the charge neutrality is said to be local. As a consequence of that, the transition is quite sharp as seen in Fig. 6-3 for zero temperature.

At the chemical potential of the phase transition, the Polyakov loop increases its value showing the deconfinement to quark matter. The chiral symmetry restoration, that in the absence of deconfinement was a smooth crossover, has a first order transition in this case. The connection is established in the dynamics of the system especially due to the shape of the potential for the Polyakov loop that contains a logarithm term [87]. The small increase in the value of the chiral condensate during the transition comes from the smaller quark baryon number (1/3) compared to the baryonic one.

The effective masses of baryons and quarks show the strict relation between these quantities (Eq. 6.5 and 6.6) and the order parameters responsible for the dynamics of the model (Fig. 6-4). In spite of taking into account all hyperons, the presence of most of them is suppressed by the appearance of quarks. In fact the only one present

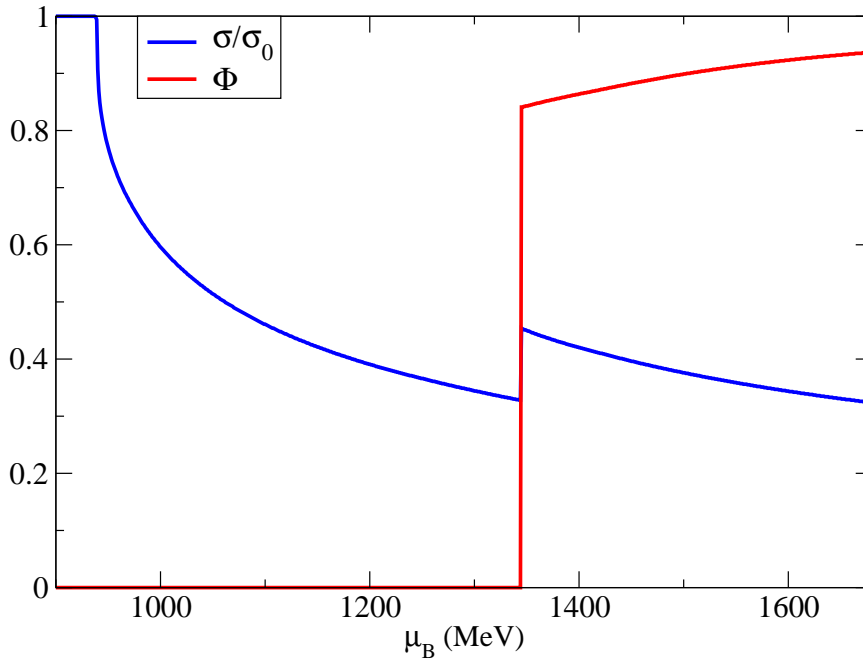


**Figure 6-3:** Order parameters for chiral symmetry restoration and deconfinement to quark matter for star matter at zero temperature.

in the hybrid star is the  $\Lambda$ . The population in the hybrid star is shown in Fig. 6-5. The density of electrons and muons is significant in the hadronic phase but not in the quark phase. The reason for this behavior is that because the down and strange quarks are also negatively charged, there is no necessity for the presence of electrons to generate charge neutrality, and only a small amount of leptons remains to assure beta equilibrium. The strange quarks appear after the other ones and do not make substantial changes in the system.

Hybrid stars are calculated using the EOS obtained from the model in the TOV equations. The solutions for hadronic (same model but without quarks) and hybrid stars are shown in Fig. 6-6, where besides our equation of state for the core, a separate equation of state was used for the crust [44]. The maximum mass supported against gravity in our model is  $2.1M_{\odot}$  in the first case and around  $2.0M_{\odot}$  in the second. Because the equation of state for the quark matter is much softer than for hadronic matter, the star becomes unstable right after the central density is higher than the phase transition threshold.

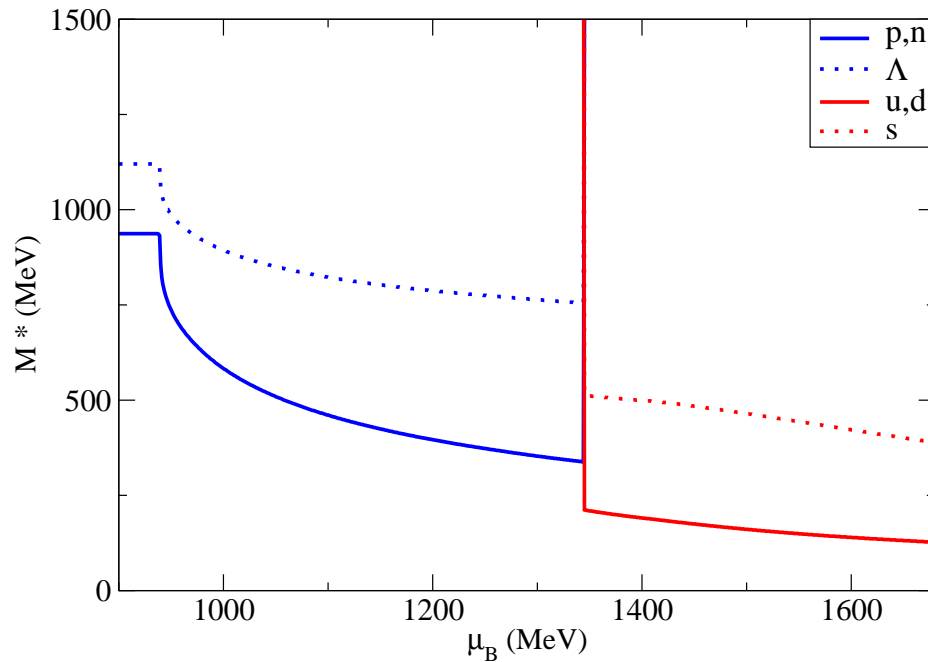


**Figure 6-4:** Effective mass of baryons and quarks for star matter at zero temperature.

### 6.4.2 Global charge neutrality

There is another option to consider for the phases in the hybrid star, called Gibbs construction [88]. If, instead of local, we consider global charge neutrality, meaning that the phases together have to be neutral, there is a mixture of phases at zero temperature. This possibility changes the particle densities in the coexistence region making them appear and vanish in a smoother way (Fig. 6-7). The mixed phase extends through a couple of kilometers of the star.

The maximum mass allowed for the star is slightly lower in the global charge neutrality case compared to the local one, as can be seen in the dotted line in Fig. 6-6. This possibility allows stable hybrid stars, but with a small amount of quarks. The mixed phase constitutes the inner core of the star up to a radius of about 2 km and there is no pure quark phase.

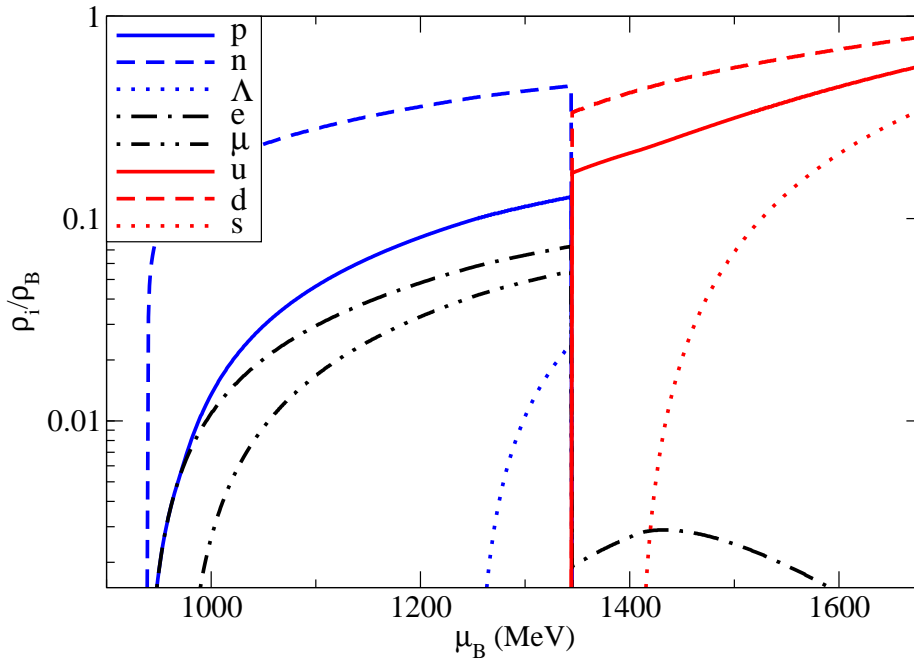


**Figure 6-5:** Population for star matter at zero temperature using local charge neutrality

## 6.5 Degrees of Freedom

During the phase transition, the change in degrees of freedom change the entropy, which is proportional to the logarithm of the number of microscopic configurations available to the system. We can make a simple estimate of the entropy change for a non-interacting gas of massless fermions. In this case the pressure is

$$P_F = \frac{g_F}{(2\pi)^3} \frac{1}{3} \int d^3k \, k \left[ \frac{1}{e^{(k_i - \mu_i)/T} + 1} + \frac{1}{e^{(k_i + \mu_i)/T} + 1} \right], \quad (6.12)$$

where particles as well as antiparticles are included and  $g_F$  is the degeneracy factor for fermions. Expanding the expression we obtain

$$P_F = \frac{7\pi^2}{360} g_F T^4 + \frac{1}{24\pi^2} g_F \mu^4 + \frac{1}{12} g_F T^2 \mu^2. \quad (6.13)$$

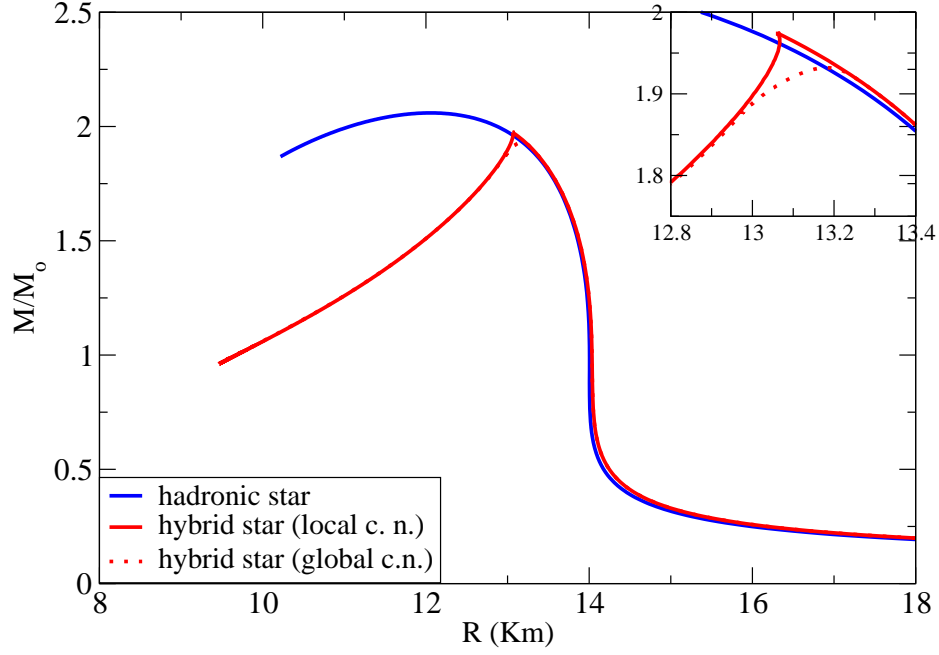


**Figure 6-6:** Mass-radius diagram for hadronic and hybrid stars at zero temperature.

For bosons the expression for pressure is analogous but we don't take anti-particles into account

$$P_B = \frac{g_B}{(2\pi)^3} \frac{1}{3} \int d^3k \, k \frac{1}{e^{(k_i - \mu_i)/T} - 1}, \quad (6.14)$$

where  $g_B$  is the degeneracy factor for bosons. Expanding the expression and using only the leading order terms we obtain

$$P_B = \frac{\pi^2}{90} g_B T^4 - \frac{1}{48\pi^2} g_B \mu^4 + \frac{1}{12} g_B T^2 \mu^2. \quad (6.15)$$

The total pressure is the sum of the pressures from the fermions and bosons  $P_T = P_F + P_B$ . The total entropy per baryon is calculated from

$$s = \frac{S}{V\rho_B} = \frac{\partial P / \partial T}{\partial P / \partial \mu}. \quad (6.16)$$

It is important to remember that in this model there is a contribution of the gluons, through the Polyakov loop to the entropy and baryon density. These contributions come from the Polyakov potential. They represent color bound states and mimic extra

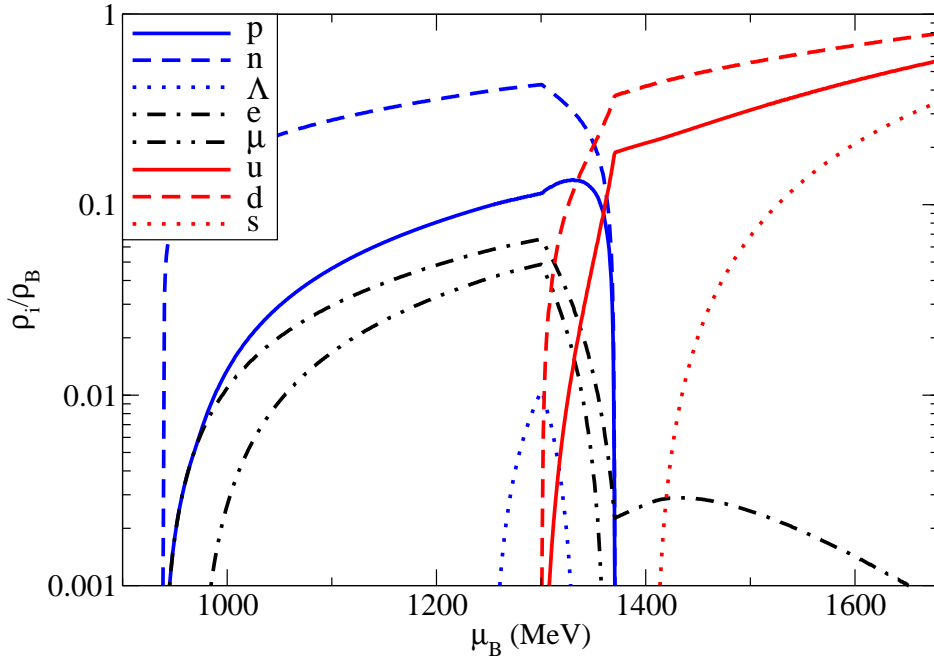


**Figure 6-7:** Population for star matter at zero temperature using global charge neutrality.

possible states, as for example the contribution of higher resonances. These loops change with the particle-antiparticle symmetry, related to the chemical potential, and the temperature. Taken the derivative of the pressure with respect to temperature and chemical potential results in

$$s = \frac{\frac{\pi^2}{15}(7/2g_F + 2g_B)T^3 + (1/2g_F + 1/2g_B)\mu^2T}{\frac{1}{\pi^2}(1/2g_F - 1/4g_B)\mu^3 + (1/2g_F + 1/2g_B)T^2\mu}, \quad (6.17)$$

which simplifies for  $\mu \gg T$  to

$$s = \pi^2 \frac{g_F + g_B}{g_F - 1/2g_B} \frac{T}{\mu}. \quad (6.18)$$

For a system of hadrons we replace the degeneracy factor  $g_B$  by zero. The resulting entropy per baryon is  $s = \pi^2 \frac{T}{\mu}$ . For a system of quarks and gluons we replace the degeneracy factor  $g_F$  by  $2N_c N_f$ , where 2 counts for spin  $\pm 1/2$ ,  $N_c$  for the number of colors and  $N_f$  for the number of quark flavors, and the degeneracy factor  $g_B$  by

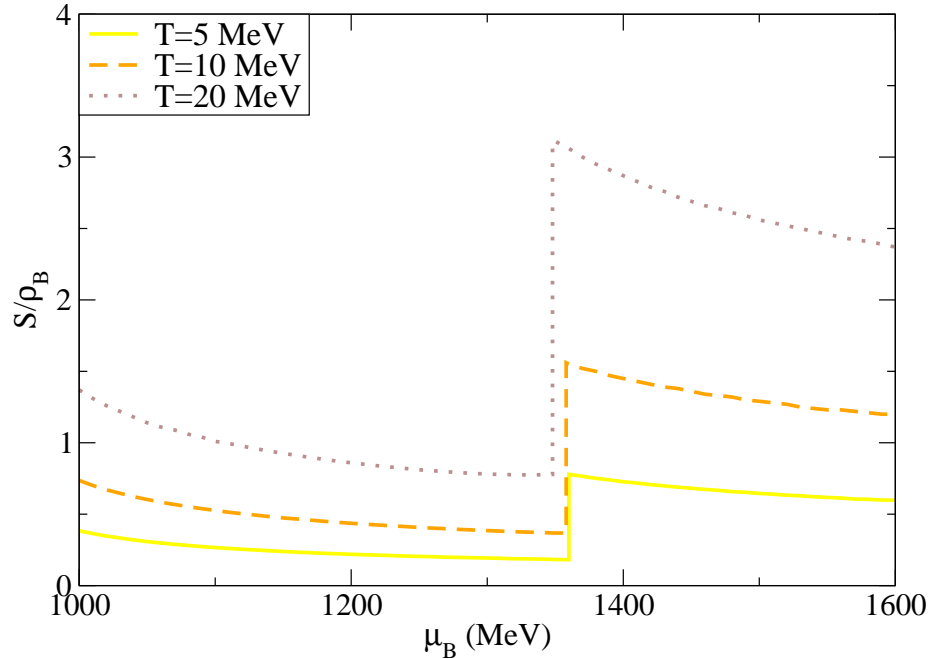


**Figure 6-8:** Entropy profile for star matter at fixed temperatures.

$2(N_c^2 - 1)$ , where 2 accounts for the different polarizations. The resulting entropy per baryon is  $s = 7\pi^2 \frac{T}{\mu}$  for  $N_c = 3$  and  $N_f = 2$ . The entropy in the quark phase is, in this simple approach, seven times the entropy in the hadronic phase.

## 6.6 Isotherms and Isentropes

As already discussed in chapter 4, neutron stars are not cold but have temperature up to tens of MeVs. Considering constant temperature hybrid stars is equivalent to looking at horizontal lines in the phase diagram 6-2. During the phase transition there is a jump in entropy shown in Fig. 6-8. In the quark phase it increases to approximately three times its value in the hadronic phase. This value has the same order of magnitude as the simple estimate from the last section, but is different due to corrections coming from finite masses and interactions.

Considering fixed entropy per baryon instead of temperature, which is a more realistic approach as already shown in chapter 4, is equivalent to looking at diagonal lines in the phase diagram. In this case, during the phase transition there is a jump in tem-



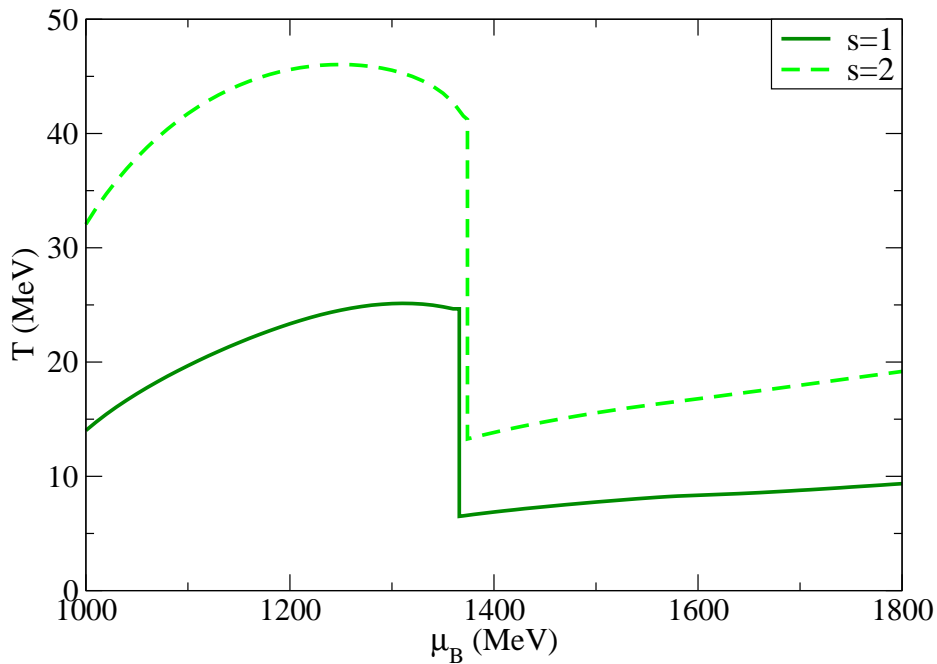


**Figure 6-9:** *Temperature profile for star matter at fixed entropies.*

perature (Fig. 6-9). The temperature reduces in the quark phase to approximately one third of its value in the hadronic phase. The small decrease of the temperature before the phase transition shows the appearance of quarks, that constitute new degrees of freedom, in the “hadronic phase”. As already mentioned, the only case where there is a pure hadronic phase and a pure quark phase is at zero temperature.

If instead of local we require global charge neutrality, the results are qualitatively the same. The jump in entropy/temperature is smoother but the entropy still increases in the first case and the temperature still decreases in the second case during the phase transitions. Because this model only allows for stable hybrid stars with mixed but not pure quark phase the results for stellar maximum masses and radii are similar to the ones for neutron stars. Consequently the constraints coming from cooling don’t change significantly in the modified chiral model compared to the one showed in the previous chapters.



## 7 Conclusion and Outlook

We used an extended  $SU(3)$  version of the sigma model adopting the non-linear realization of chiral symmetry to study neutron stars. Firstly, we changed the original couplings and parameters from the original model [12]. Choosing between the possible chiral invariants for the self interaction of the vector mesons, we concluded that the one without mixing between the vector-isoscalar and the vector-isovector mesons allows more massive neutron stars. Applying the mean-field approximation and solving the TOV equations for charge neutral matter in beta equilibrium we obtained high neutron star maximum masses even for stars containing higher degrees of freedom, as hyperons or higher resonances. Although the new degrees of freedom make the EOS softer, the star maximum masses are still above the limit of  $1.74M_{\odot}$  [48]. In practice, the only baryons present in the star besides the nucleons are the  $\Lambda$  and  $\Sigma^{-}$  in the first case and  $\Lambda$  and  $\Delta^{-,0,+,++}$  resonances in the second case. We choose to proceed with our calculations including the baryon octet but not the spin 3/2 baryonic decuplet, in order to avoid uncertainties in the meson couplings to these particles. The couplings of the hyperons were fitted to the depth of their potentials.

Through the analysis of the related order parameter, we saw that the chiral symmetry begins to be restored inside neutron stars. The transition is a smooth crossover for any possible coupling, composition or temperature. Although the chiral condensate decreases its value, thereby decreasing the masses of the baryons, it does not go to zero, which is a consequence of the shape of the potential of the scalar mesons.

In order to model proto-neutron stars, we included finite temperature and trapped neutrinos in the model. Finite-temperature calculations included the heat bath of hadronic quasiparticles within the grand canonical potential of the system. Different schemes were considered, with constant temperature, metric dependent temperature and constant entropy, the latter one being the most realistic approach. In this case the temperature increases substantially with density reaching 50 MeV in the core of the star. While the rise in temperature increases the respective neutron star mass, due to thermal effects on the binding part of it, the presence of neutrinos decreases it.

The neutrino chemical potential was introduced by fixing the lepton number. It also controls the amount of electrons and protons (for charge neutrality), and the higher the amount of protons in the star compared to neutrons, the lower is the Fermi energy. The balance between these two features is delicate and influenced mainly by the baryonic number conservation. Fixing the baryon number to the one allowed in the first stage of the cooling created constraints on the maximum masses allowed for neutron star in the last stage, the deleptonized cold star. Following this procedure, we concluded that the maximum mass of the stars decreased with time.

The inclusion of rotational effects allowed more massive neutron stars, although this effect was not very substantial due to the baryon number constraint. While a star accreting mass from a companion could increase its mass due to rotation by 15%, an isolated star could only gain 5%. If a second constraint was made on the angular momentum during the cooling, instability windows showed up. Fast rotating stars with high baryon number can exist but cannot stably spin down. They necessarily collapse to black holes.

The model was modified to include quark degrees of freedom. The Polyakov loop was used as the order parameter for deconfinement. We fitted its potential and coupling constants in order to reproduce, besides lattice QCD results, neutron star properties. We did that by introducing a new dependence on the chemical potential in the Polyakov potential. With this we were able to obtain the QCD phase diagram with a crossover region and a first order transition line separated by a critical point. The critical point was situated at  $\mu_{Bc} = 354$  MeV and  $T_c = 167$  MeV for symmetric matter (in accordance with [86]). The critical temperatures for chiral symmetry restoration coincided with the ones from deconfinement. Each phase contained hadrons and quarks in higher or lower quantity but for the zero temperature case, in which there was no mixing for any density. For star matter the first order transition line ended at the zero temperature axis at  $\mu_B = 1345$  MeV, that is equivalent to four times saturation density.

We calculated hybrid stars using local charge neutrality. In this approach the stars became unstable right after deconfinement. In a second approach we used global charge neutrality. It generated stable stars that contained a mixed phase of hadrons and quarks but no pure quark phase. The mixed phase occupied the inner 2 km of the star. The maximum masses and radius of the hybrid stars did not differ much from the neutron stars.

---

Considerations of finite temperature and entropy in hybrid stars were done with local charge neutrality. They showed a jump in the temperature during the phase transition. If we had used global charge neutrality instead, the results would be qualitative the same. The jump in temperature would have been smoother but the temperature would still have decreased in the quark phase compared to the hadronic one. Because this model only allowed stable hybrid stars with mixed but not pure quark phase the constraints coming from cooling did not change significantly compared to the model showed in the first chapters.

With the modified chiral model working, in the future we intend to study different couplings of the Polyakov loop to the effective mass of the baryons and quarks to verify if there is a possibility of obtaining hybrid stars with pure quark matter. In this case it would be interesting to see how the phase transition to deconfined matter affects the cooling of the star. For example, the measurement of the braking index, related to the change in the angular velocity of the star, could give experimental evidence for a phase transition to deconfined matter inside hybrid stars [89, 90].

We also want to investigate the effect of the Polyakov loop when it is not equal to its conjugate  $\Phi^* \neq \Phi$ . This might have interesting effects at high chemical potential. Another possibility is the investigation of the effect of the introduction of a color chemical potential in the model in order to conserve color neutrality. As suggested by [91, 92], the Wilson lines couple to each color with a different weight, making the energy required to populate red and green quarks different from the one to populate the blue ones. This might change the temperature for deconfinement and the position of the critical point.

A major advantage of our work compared to other studies of hybrid stars is that because we have only one equation of state for different degrees of freedom we can study in detail the way in which chiral symmetry is restored and the way deconfinement occurs at high temperature/density. Since the properties of the physical system, as for example the density of particles in each phase, are directly connected to the Polyakov loop it is not surprising that we obtain different results in a combined description of the degrees of freedom compared to a simple connection of two separate equations of state.

Since the model additionally shows a realistic structure of the phase transition over the whole range of chemical potentials and temperatures as well as phenomenologically

acceptable results for saturated nuclear matter, this approach presents an ideal tool for the study of ultrarelativistic heavy-ion collisions. The use of the EOS of the modified chiral model in hydrodynamic calculations showed values for observables such as the speed of sound  $v_c$  and the  $V_1$ , related to the anisotropy of the system, in accordance with heavy-ion collision measurements. Calculations along this line are in progress [93].

## 8 Appendix

### Hadronic Multiplets

Scalar, vector and baryonic matrices with Lorentz index suppressed

$$X = \begin{pmatrix} \frac{\delta^0 + \sigma}{\sqrt{2}} & \delta^+ & k^+ \\ \delta^- & \frac{-\delta^0 + \sigma}{\sqrt{2}} & k^0 \\ k^- & \bar{k}^0 & \zeta \end{pmatrix} \quad (8.1)$$

$$V = \begin{pmatrix} \frac{\rho_0^0 + \omega}{\sqrt{2}} & \rho_0^+ & k^{*+} \\ \rho_0^- & \frac{-\rho_0^0 + \omega}{\sqrt{2}} & k^{*0} \\ k^{*-} & \bar{k}^{*0} & \phi \end{pmatrix} \quad (8.2)$$

$$B = \begin{pmatrix} \frac{\Sigma^0}{\sqrt{2}} + \frac{\Lambda^0}{\sqrt{6}} & \Sigma^+ & p \\ \Sigma^- & -\frac{\Sigma^0}{\sqrt{2}} + \frac{\Lambda^0}{\sqrt{6}} & n \\ \Xi^- & \Xi^0 & -2\frac{\Lambda^0}{\sqrt{6}} \end{pmatrix} \quad (8.3)$$





## References

- [1] K. Schwarzschild, Sitzungsber. Preuss. Akad. Wiss. Berlin (Math. Phys. ) **1916** (1916) 189 [arXiv:physics/9905030].
- [2] A. Hewish, S. J. Bell, J. D. H. Pilkington, P. F. Scott and R. A. Collins, Nature **217**, 709 (1968).
- [3] J. W. T. Hessels, S. M. Ransom, I. H. Stairs, P. C. C. Freire, V. M. Kaspi and F. Camilo, arXiv:astro-ph/0601337.
- [4] M. Kramer *et al.*, Science **314**, 97 (2006) [arXiv:astro-ph/0609417].
- [5] G. W. Collins, W. P. Claspy and J. C. Martin, arXiv:astro-ph/9904285.
- [6] G. Goldhaber *et al.* [The Supernova Cosmology Project Collaboration], arXiv:astro-ph/0104382.
- [7] J. H. Jeans, Philosophical Transactions of the Royal Society of London A **199**, 1 (1902).
- [8] A. Sulaksono, C. Kalempouw-Williams, P. T. P. Hutauruk and T. Mart, Phys. Rev. C **73**, 025803 (2006) [arXiv:nucl-th/0601002].
- [9] R. C. Tolman, Phys. Rev. **55** (1939) 364.
- [10] J. R. Oppenheimer and G. M. Volkoff, Phys. Rev. **55**, 374 (1939).
- [11] N. K. Glendenning and F. Weber, Phys. Rev. D **50**, 3836 (1994).
- [12] P. Papazoglou, D. Zschesche, S. Schramm, J. Schaffner-Bielich, H. Stoecker and W. Greiner, Phys. Rev. C **59**, 411 (1999) [arXiv:nucl-th/9806087].
- [13] J. D. Walecka, Annals Phys. **83**, 491 (1974).
- [14] D. J. Gross and F. Wilczek, Phys. Rev. Lett. **30**, 1343 (1973).

- [15] D. J. Gross and F. Wilczek, *Phys. Rev. D* **8**, 3633 (1973).
- [16] J. O. Andersen and M. Strickland, *Annals Phys.* **317**, 281 (2005) [arXiv:hep-ph/0404164].
- [17] J. P. Blaizot, E. Iancu and A. Rebhan, *Phys. Rev. D* **68**, 025011 (2003) [arXiv:hep-ph/0303045].
- [18] B. Freedman and L. D. McLerran, *Phys. Rev. D* **17**, 1109 (1978).
- [19] J. B. Kogut, *Rev. Mod. Phys.* **55**, 775 (1983).
- [20] J. M. Maldacena, *Adv. Theor. Math. Phys.* **2**, 231 (1998) [*Int. J. Theor. Phys.* **38**, 1113 (1999)] [arXiv:hep-th/9711200].
- [21] E. Witten, *Adv. Theor. Math. Phys.* **2**, 253 (1998) [arXiv:hep-th/9802150].
- [22] S. S. Gubser, I. R. Klebanov and A. M. Polyakov, *Phys. Lett. B* **428**, 105 (1998) [arXiv:hep-th/9802109].
- [23] H. Leutwyler, *Annals Phys.* **235**, 165 (1994) [arXiv:hep-ph/9311274].
- [24] Y. Nambu and G. Jona-Lasinio, *Phys. Rev.* **122**, 345 (1961).
- [25] Y. Nambu and G. Jona-Lasinio, *Phys. Rev.* **124**, 246 (1961).
- [26] E. Noether, *Nachr. D. Knig. Gesellsch. D. Wiss. Zu Gttingen, Math-phys. Klasse* 1918, 235 (1918).
- [27] P. Papazoglou, S. Schramm, J. Schaffner-Bielich, H. Stoecker and W. Greiner, *Phys. Rev. C* **57**, 2576 (1998) [arXiv:nucl-th/9706024].
- [28] J. T. Lenaghan, D. H. Rischke and J. Schaffner-Bielich, *Phys. Rev. D* **62**, 085008 (2000) [arXiv:nucl-th/0004006].
- [29] S. Weinberg, *Phys. Rev. Lett.* **18**, 188 (1967).
- [30] S. R. Coleman, J. Wess and B. Zumino, *Phys. Rev.* **177**, 2239 (1969).
- [31] C. G. Callan, S. R. Coleman, J. Wess and B. Zumino, *Phys. Rev.* **177**, 2247 (1969).

- [32] S. Weinberg, *Cambridge, UK: Univ. Pr. (1996) 489 p*
- [33] D. Zschesche, P. Papazoglou, S. Schramm, J. Schaffner-Bielich, H. Stoecker and W. Greiner, *Phys. Rev. C* **63**, 025211 (2001) [arXiv:nucl-th/0001055].
- [34] J. J. Sakurai, *Currents and mesons*, University of Chicago Press, Chicago, 1969.
- [35] J. Schechter, *Phys. Rev. D* **21**, 3393 (1980).
- [36] L. Bonanno and A. Drago, arXiv:0805.4188 [nucl-th].
- [37] P. Papazoglou. Einheitliche Beschreibung von Hadronen und Kernen in einen chiralen SU(3)-Model, Dissertation, J. W. Goethe Universtitaet. Frankfurt am Main, 1998.
- [38] E. K. Heide, S. Rudaz and P. J. Ellis, *Nucl. Phys. A* **571**, 713 (1994) [arXiv:nucl-th/9308002].
- [39] S. Gasiorowicz and D. A. Geffen, *Rev. Mod. Phys.* **41**, 531 (1969).
- [40] P. K. Mitter and L. J. Swank, *Nucl. Phys. B* **8**, 205 (1968).
- [41] B. D. Serot and J. D. Walecka, *Int. J. Mod. Phys. E* **6**, 515 (1997) [arXiv:nucl-th/9701058].
- [42] D. G. Yakovlev and C. J. Pethick, *Ann. Rev. Astron. Astrophys.* **42**, 169 (2004) [arXiv:astro-ph/0402143].
- [43] L. Frankfurt, M. Sargsian and M. Strikman, *Int. J. Mod. Phys. A* **23**, 2991 (2008) [arXiv:0806.4412 [nucl-th]].
- [44] G. Baym, C. Pethick and P. Sutherland, *Astrophys. J.* **170**, 299 (1971).
- [45] T. K. Jha, H. Mishra and V. Sreekanth, *Phys. Rev. C* **77**, 045801 (2008) [arXiv:0710.5392 [nucl-th]].
- [46] J. Schaffner and I. N. Mishustin, *Phys. Rev. C* **53**, 1416 (1996) [arXiv:nucl-th/9506011].

- [47] M. Hanauske, D. Zschesche, S. Pal, S. Schramm, H. Stoecker and W. Greiner, arXiv:astro-ph/9909052.
- [48] D. J. Champion *et al.*, arXiv:0805.2396 [astro-ph].
- [49] D. Zschesche, G. Zeeb and S. Schramm, J. Phys. G **34**, 1665 (2007) [arXiv:nucl-th/0602073].
- [50] G. F. Marranghello, C. A. Z. Vasconcellos and M. Dillig, Int. J. Mod. Phys. E **11**, 83 (2002) [arXiv:astro-ph/0107476].
- [51] D. Gondek, P. Haensel and J. L. Zdunik, Astron. Astrophys. **325**, 217 (1997) [arXiv:astro-ph/9705157].
- [52] J. Stein and J. C. Wheeler, Astrophys. J. **643**, 1190 (2006) [arXiv:astro-ph/0512580].
- [53] J. A. Pons, S. Reddy, M. Prakash, J. M. Lattimer and J. A. Miralles, Astrophys. J. **513**, 780 (1999) [arXiv:astro-ph/9807040].
- [54] J. A. Pons, J. A. Miralles, M. Prakash and J. M. Lattimer, Astrophys. J. **553**, 382 (2001) [arXiv:astro-ph/0008389].
- [55] J. A. Pons, A. W. Steiner, M. Prakash and J. M. Lattimer, Phys. Rev. Lett. **86**, 5223 (2001) [arXiv:astro-ph/0102015].
- [56] I. Bednarek and R. Manka, Phys. Rev. C **73**, 045804 (2006) [arXiv:nucl-th/0601022].
- [57] T. Takatsuka, Nucl. Phys. A **588**, 365 (1995).
- [58] M. Bagchi, S. Ray, M. Dey and J. Dey, Astron. Astrophys. **450**, 431 (2006) [arXiv:astro-ph/0601282].
- [59] M. Bagchi, R. Ouyed, J. Staff, S. Ray, J. Dey and M. Dey, Mon. Not. Roy. Astron. Soc. **387**, 115 (2008) [arXiv:astro-ph/0607509].
- [60] J. M. Lattimer and F. D. Westy, Nucl. Phys. A **535**, 331 (1991).

- [61] O. E. Nicotra, arXiv:nucl-th/0607055.
- [62] K. Strobel, C. Schaab and M. K. Weigel, *Astron. Astrophys.* **350**, 497 (1999) [arXiv:astro-ph/9908132].
- [63] A. J. Faulkner *et al.*, *Astrophys. J.* **618**, L119 (2004) [arXiv:astro-ph/0411796].
- [64] S. N. Bose, *Zeitschrift fr Physik* **26**, 178 (1924).
- [65] A. Einstein, *Sitzungsberichte der Preussischen Akademie der Wissenschaften* **1**, 3 (1925).
- [66] A. Mishra, A. Kumar, S. Sanyal and S. Schramm, arXiv:0808.1937 [nucl-th].
- [67] A. Mishra, S. Schramm and W. Greiner, *Phys. Rev. C* **78**, 024901 (2008) [arXiv:0802.0363 [nucl-th]].
- [68] J. A. Pons, S. Reddy, P. J. Ellis, M. Prakash and J. M. Lattimer, *Phys. Rev. C* **62**, 035803 (2000) [arXiv:nucl-th/0003008].
- [69] S. Banik and D. Bandyopadhyay, *Phys. Rev. C* **63**, 035802 (2001) [arXiv:astro-ph/0009113].
- [70] S. Schramm and D. Zschesche, *J. Phys. G* **29**, 531 (2003).
- [71] J. B. Hartle and K. S. Thorne, *Astrophys. J.* **153**, 807 (1968).
- [72] P. Kaaret *et al.*, arXiv:astro-ph/0611716.
- [73] N. Stergioulas and J. L. Friedman, *Astrophys. J.* **444**, 306 (1995)
- [74] J. O. Goussard, P. Haensel and J. L. Zdunik, *Astron. Astrophys.* **330**, 1005 (1998) [arXiv:astro-ph/9711347].
- [75] N. Itoh, *Prog. Theor. Phys.* **44**, 291 (1970).
- [76] N. K. Glendenning, F. Weber and S. A. Moszkowski, *Phys. Rev. C* **45**, 844 (1992).
- [77] F. Weber and M. K. Weigel, *Nucl. Phys. A* **505**, 779 (1989).

- [78] G. W. Carter, P. J. Ellis and S. Rudaz, Nucl. Phys. A **603**, 367 (1996) [Erratum-  
ibid. A **608**, 514 (1996)] [arXiv:nucl-th/9512033].
- [79] F. Weber, Prog. Part. Nucl. Phys. **54**, 193 (2005) [arXiv:astro-ph/0407155], and  
references therein.
- [80] M. Buballa, Phys. Rept. **407**, 205 (2005) [arXiv:hep-ph/0402234].
- [81] H. Heiselberg, C. J. Pethick and E. F. Staubo, Phys. Rev. Lett. **70**, 1355 (1993).
- [82] K. Fukushima, Phys. Lett. B **591**, 277 (2004) [arXiv:hep-ph/0310121].
- [83] S. Roessner, T. Hell, C. Ratti and W. Weise, Nucl. Phys. A **814**, 118 (2008)  
[arXiv:0712.3152 [hep-ph]].
- [84] C. Ratti, M. A. Thaler and W. Weise, Phys. Rev. D **73**, 014019 (2006)
- [85] S. Roszner, C. Ratti and W. Weise, Phys. Rev. D **75**, 034007 (2007)
- [86] Z. Fodor and S. D. Katz, JHEP **0404**, 050 (2004) [arXiv:hep-lat/0402006].
- [87] W. j. Fu, Z. Zhang and Y. x. Liu, Phys. Rev. D **77**, 014006 (2008)  
[arXiv:0711.0154 [hep-ph]].
- [88] N. K. Glendenning, Phys. Rev. D **46**, 1274 (1992).
- [89] N. K. Glendenning, S. Pei and F. Weber, Phys. Rev. Lett. **79**, 1603 (1997)  
[arXiv:astro-ph/9705235].
- [90] H. Heiselberg and M. Hjorth-Jensen, Phys. Rev. Lett. **80**, 5485 (1998)  
[arXiv:astro-ph/9801187].
- [91] H. Abuki, M. Ciminale, R. Gatto, G. Nardulli and M. Ruggieri, Phys. Rev. D **77**,  
074018 (2008) [arXiv:0802.2396 [hep-ph]].
- [92] D. Gomez Dumm, D. B. Blaschke, A. G. Grunfeld and N. N. Scoccola, Phys. Rev.  
D **78**, 114021 (2008) [arXiv:0807.1660 [hep-ph]].
- [93] S. Schramm, J. Steinheimer, and V. Dexheimer, in preparation.

## List of Figures

0-1	Links: Masse-Radius-Diagramm fuer Sterne mit verschiedenen baryonischen Freiheitsgraden (gezeigt werden die Werte der jeweiligen hoechsten Masse). Rechts: Skalares Kondensat gegen den Radius des Sterns.	5
0-2	Links: Masse des Sterns in verschiedenen Phasen der Sternentwicklung, definiert durch die Entropie und die Leptonenzahl unter Beruecksichtigung des Baryonen-Oktetts, $e$ , $\mu$ . Rechts: Phasendiagramm der Materie in der Ebene von Temperatur und baryonischen chemischen Potential, die Linien repraesentieren Phasenuebergaeunge erster Ordnung fuer isospin-symmetrische und Sternenmaterie, die Kreise markieren die jeweiligen kritischen Punkte. . . . .	6
1-1	Pulsar mechanism . . . . .	14
1-2	Crab nebula . . . . .	15
1-3	Main sequence star structure . . . . .	16
3-1	Star masses versus radii for different vector meson self-interactions. The values of the respective maximum masses are shown. . . . .	46
3-2	The composition of neutron star matter with hyperons. . . . .	47
3-3	The composition of neutron star matter with hyperons and resonances. . . . .	48
3-4	Binding energy per nucleon versus baryon density for different compositions. . . . .	49
3-5	Star mass versus radius for different compositions. The values of the respective maximum masses are shown. . . . .	50
3-6	Normalized scalar condensate versus star radius. . . . .	50
4-1	Entropy per baryon versus baryon density for different temperatures. . . . .	53
4-2	Scalar condensate versus chemical potential for different temperatures. . . . .	54
4-3	Temperature versus baryon density for $T_\infty = 15$ MeV. . . . .	55
4-4	Temperature versus baryon density for different entropies per volume per baryon. . . . .	56

4-5	Star mass versus radius for different stages of the star evolution defined by temperature and lepton number considering the baryon octet, $e$ , $\mu$ . . . . .	58
4-6	Star mass versus radius for different stages of the star evolution defined by entropy and lepton number considering the baryon octet, $e$ , $\mu$ . . . . .	59
5-1	Star mass versus rotational frequency with and without fixing the baryonic number. . . . .	66
6-1	Order parameters for chiral symmetry restoration and deconfinement to quark matter for symmetric matter at zero chemical potential. . . . .	72
6-2	Phase diagram. The lines represent first order transitions for symmetric and star matter. The circles mark the respective critical end-points. . . . .	73
6-3	Order parameters for chiral symmetry restoration and deconfinement to quark matter for star matter at zero temperature. . . . .	75
6-4	Effective mass of baryons and quarks for star matter at zero temperature. . . . .	76
6-5	Population for star matter at zero temperature using local charge neutrality . . . . .	77
6-6	Mass-radius diagram for hadronic and hybrid stars at zero temperature. . . . .	78
6-7	Population for star matter at zero temperature using global charge neutrality. . . . .	79
6-8	Entropy profile for star matter at fixed temperatures. . . . .	80
6-9	Temperature profile for star matter at fixed entropies. . . . .	81



## List of Tables

- 4-1 Maximum masses with and without fixing the baryon number, radii for the maximum masses with fixed baryon number and minimum masses with and without fixing the baryon number for different moments of the star evolution. . . . . 57
- 5-1 Maximum frequencies and masses with and without fixing  $M_B$  and  $L$  for different stages of the cooling. . . . . 67



## Acknowledgments

I would like to thank firstly my adviser Stefan Schramm for the constant support and unlimited patience with my problems. I would also like to acknowledge Horst Stoecker and all the people that made FIAS possible. Without any doubt, my work was highly influenced by the interesting and stimulating environment of the institute. I appreciate all the support given by my friends specially Graziela Grise, Mauricio Martinez, Nan Su and Michael Strickland who helped me survive through the last year. Finally I would like to thank Juergen Schaffner, Mathias Hempel and all the astrophysics group for the numerous discussions.



# Publications

## Articles

**1)** A Novel Approach to Model Hybrid Stars.

V.A. Dexheimer, S. Schramm . Jan 2009.

e-Print: arXiv:0901.1748[astro-ph]

**2)** Neutron stars within the SU(2) parity doublet model.

V. Dexheimer, G. Pagliara , L. Tolos, J. Schaffner-Bielich, S. Schramm. May 2008.

Accepted for publication in The European Physical Journal A.

e-Print: arXiv:0805.3301[nucl-th]

**3)** Proto-Neutron and Neutron Stars in a Chiral SU(3) Model.

V. Dexheimer, S. Schramm. Feb 2008.

Published in Astrophys.J.683:943?948,2008.

**4)** Nuclear matter and neutron stars in a parity doublet model.

V. Dexheimer, S. Schramm, D. Zschesche. Oct 2007.

Published in Phys.Rev.C77:025803,2008.

**5)** Density Dependent Nuclear Matter Compressibility.

V.A. Dexheimer, C.A.Z. Vasconcellos, B.E.J. Bodmann. Feb 2007. 6pp.

Published in Phys.Rev.C 77:065803,2008

## Proceedings

**1)** Neutron Stars as a Probe for Dense Matter.

V. Dexheimer, S. Schramm . Dec 2008.

Prepared for International Conference on Particles And Nuclei (PANIC08), Eilat, Israel, 9-14 Nov 2008.

e-Print: arXiv:0812.0247[astro-ph]

**2)** Proto-Neutron and Neutron Stars.

V. Dexheimer, S. Schramm, H. Stcker . Jan 2008.

Prepared for International Workshop on Astronomy and Relativistic Astrophysics (IWARA 2007), Joao Pessoa, Brazil, 3-6 Oct 2007.

Accepted for publication in Int.J.Mod.Phys.D.

e-Print: arXiv:0801.2523[astro-ph].

**3) Parity Doublet Model applied to Neutron Stars.**

V. Dexheimer, S. Schramm, Horst Stoecker. Oct 2007.

To appear in the proceedings of EXOCT 2007: International Symposium on Exotic States of Nuclear Matter, Catania, Italy, 11-15 Jun 2007.

e-Print: arXiv:0710.3067[astro-ph].

**4) Neutron Stars in a Chiral Model with Finite Temperature.**

V. Dexheimer, S. Schramm, H. Stoecker. Aug 2007.

Prepared for 3rd Nuclear Physics in Astrophysics Conference and 21st International Nuclear Physics Divisional Conference of the European Physical Society, Dresden, Germany, 26-31 Mar 2007.

Published in J.Phys.G35:014060,2008.

**5) The Nuclear matter compressibility function in a parameterized coupling model.**

Veronica A. Dexheimer, Cesar A.Z. Vasconcellos, Bardo E.J. Bodmann. Feb 2007.

Prepared for International Workshop on Astronomy and Relativistic Astrophysics (IWARA 2005), Natal, Brazil, 2-5 Oct 2005.

Published in Int.J.Mod.Phys.D16:269-376,2007.

**6) The role of the nuclear incompressibility in a relativistic mean field theory for neutron stars.**

V.A. Dexheimer, C.A.Z. Vasconcellos, B.E.J. Bodmann, M. Dillig. 2005.

Prepared for 9th Hadron Physics and 7th Relativistic Aspects of Nuclear Physics, Angra dos Reis, Rio de Janeiro, Brazil, 28 Mar - 3 Apr 2004.

Published in AIP Conf.Proc.739:479-481,2005.

**7) The Role of the nuclear matter compression modulus in neutron stars.**

V.A. Dexheimer, C.A.Z. Vasconcellos, M. Razeira, M. Dillig. Aug 2004.

Prepared for International Workshop on Astronomy and Relativistic Astrophysics (IWARA 2003), Olinda, Brazil, 12-16 Oct 2003.

Published in Int.J.Mod.Phys.D13:1519-1524,2004.

# Curriculum Vitae

## Personal Data

Name: Veronica Antocheviz Dexheimer

Date of Birth: 06/24/1981

Place: Porto Alegre, Rio Grande do Sul, Brasil

Nationality: Brazilian

Languages: Portuguese, Spanish, English, German

## Contact Information

Frankfurt Institute for Advanced Studies

Johann Wolfgang Goethe University

Ruth-Moufang-Str. 1

60438 Frankfurt am Main

Germany

Telephone: +49 (69) 798 47520

E-mail: dexheimer@th.physik.uni-frankfurt.de

## Education

- 1988 - 1995

Elementary School

Instituicao Superior de Educacao Sevigne ? Porto Alegre, Rio Grande do Sul, Brasil

- 1996 - 1998

High School

Colegio Leonardo da Vinci Beta ? Porto Alegre, Rio Grande do Sul, Brasil

- 1999 - 2003

B.A. Physics

Universidade Federal do Rio Grande do Sul ? Porto Alegre, Rio Grande do Sul, Brasil

- 2003 - 2006

M.A. Physics

Advisers: Cesar Vasconcellos and Bardo Bodmann

Thesis: Nuclear Matter Compressibility in Neutron Stars

Universidade Federal do Rio Grande do Sul ? Porto Alegre, Rio Grande do Sul, Brasil

Scholarship: CAPES

- 2006 - 2009

Ph.D. Physics

Advisers: Stefan Schramm and Horst Stoecker

Frankfurt Institute for Advanced Studies, Johann Wolfgang Goethe University - Frankfurt an Main, Germany

Scholarship: Buchmann Foundation

## Research Interests

Nuclear Physics

Astrophysics

High Energy and Heavy Ion Physics